Diamond & Related Materials 143 (2024) 110866

Contents lists available at ScienceDirect

Diamond & Related Materials

journal homepage: www.elsevier.com/locate/diamond

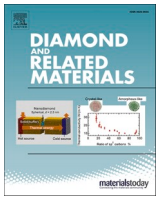

Hydrogen-related defects in diamond: A comparison between observed and calculated FTIR spectra

Maxwell C. Day [a,*], Michael C. Jollands [b], Davide Novella [a], Fabrizio Nestola [a], Roberto Dovesi [c], Martha G. Pamato [a]

[a] Dipartimento di Geoscienze, Università degli Studi di Padova, Via Gradenigo 6, I-35131 Padova, Italy
[b] Gemological Institute of America (GIA), 50 W 47th St., New York, NY 10036, USA
[c] Accademia delle Scienze di Torino, Via Accademia delle Scienze 6, 10123 Torino, Italy

ARTICLE INFO

Keywords:
Diamond
FTIR spectroscopy
Hydrogen defects
N-aggregation
Vibrational modes
Ab-initio simulations

ABSTRACT

A comprehensive and up-to-date compilation of observed and calculated hydrogen (H)-related peaks that occur in the near- and middle-infrared spectra of diamond is presented. The experimental database contains >300 observed peaks attributed to H-related impurities in natural diamond. The database of calculated peaks includes data from first-principles simulations of the FTIR spectra of different $V_xN_yH_z$ defects in diamond and contains >300 peaks that correspond to different C-H, N-H, and B-H vibrational modes for each $V_xN_yH_z$ defect. Less than ~10 % of observed H-related peaks have been assigned to specific defects. Consequently, the computational database was constructed to better understand the properties of different $V_xN_yH_z$ defects that may correspond to different observed peaks. In general, hydrogen-rich diamonds with a dominant *Type Ib* character and thus poorly aggregated N, show a larger number of low-intensity, H-related peaks compared to diamonds with a dominant *Type Ia* character. For example, ~51 % of observed H-related peaks are only observed in *Type Ib* diamonds, ~9 % of peaks are only observed in diamonds with a dominant *Type Ia* character and ~40 % of peaks are observed in both *Type Ia* and *Type Ib* diamonds. There is a major increase in the number of distinct H-related peaks in *Type IaA + Ib* diamonds compared to *Type Ib* diamonds suggesting N-aggregation processes responsible for the formation of A-centers may also produce many distinct $V_xN_yH_z$ defects capable of trapping H. There is a major decrease in the number of H-related peaks in *Type IaA > Ib* diamonds compared to *Type IaA + Ib* diamonds suggesting that many of the $V_xN_yH_z$ defects associated with the initial production of A-centers become unstable with increasing mantle residence time and the progressive loss of C-centers. These defects likely combine (or disaggregate and then re-combine) to form fewer, relatively more intense, H-related peaks observed in *Type IaA > Ib* diamonds. Many of these peaks persist through continued annealing in the mantle and are observed in *Type IaA*, *IaAB*, and *IaB* diamonds. Our data suggests that N and H incorporation are not correlated during diamond growth and that in the early stages of diamond residence, H is incorporated into many distinct $V_xN_yH_z$ defects that involve C- and A-centers. With continued residence and annealing, and the progressive formation A-centers and loss of C-centers, these defects aggregate to form relatively fewer, presumably more stable, $V_xN_yH_z$ defects such as VN_3H.

1. Introduction

Apart from nitrogen (N), hydrogen (H) is the most ubiquitous chemical impurity in natural diamond and synthetic diamonds grown at high pressure and high temperature (HPHT) or by chemical vapor deposition (CVD). The concentration and local bonding environment of H may strongly affect the properties of its host diamond such as color, luminescence (*e.g.* [1]), growth (morphology and zonation, *e.g.* [2]) and the formation and evolution of many different point- and extended-defects related to extrinsic imperfections (impurities such as N and B (boron), see *e.g.*, [3]). Hydrogen in diamond offers a unique and powerful proxy through which we can better understand (1) coupled N/H-aggregation processes and their effect on estimations of mantle residence times and temperatures; (2) mechanisms by which impurities

* Corresponding author.
E-mail address: maxwell.day@unipd.it (M.C. Day).

https://doi.org/10.1016/j.diamond.2024.110866
Received 27 November 2023; Received in revised form 8 January 2024; Accepted 24 January 2024
Available online 29 January 2024

such as N and H are incorporated during diamond nucleation and growth; (3) controls on the morphology (*e.g.* cuboid *vs.* octahedral diamond) and the rate of diamond growth; and (4) sources of recycled and primordial diamond forming media (*e.g.,* aqueous C-O-H fluids) by H isotopic analysis. However, to address such questions, one must first be able to reliably and efficiently quantify the concentration and spatial distribution of H in diamond.

Nuclear reaction analysis (NRA) of natural diamond has revealed H contents of 500–3500 at.ppm [4] up to 7000 at.ppm [5,6], while ion-beam spectrochemical analyses (IBSCA) yield H concentrations up to 1 at.% [7]. However, both NRA and IBSCA are surface techniques capable of measuring H contents down to depths of only ~200 nm or less [8,9] and thus are subject to problems related to surface adsorption of H [5]. Elastic recoil detection analysis (ERDA) [10] is also a surface technique capable of measuring H contents down to similar depths and may also be used to determine the 3D distribution of H in diamond (see *e.g.*, [11–13]). The high spatial resolution of ERDA has allowed for more precise differentiation of H-contents representative of surface adsorbed H and bulk H contents (*e.g.* [14,15]) compared to the other surface techniques and is a more reliable method for the bulk determination of H in diamond. Nanoscale secondary ion mass spectrometry (NanoSIMS) has seen considerable use for the determination of H content in natural and synthetic diamond (*e.g.* [16,17]) due to its relatively high precision and low detection limits. However, the use of NanoSIMS requires that one overcomes several difficulties related to the calibration of diamond standards with known H content, and accounting for surface contamination by H and H gas in the vacuum environment [16,18]. Bulk techniques such as proton-proton scattering (PPS) (*e.g.* [9,19]) can also be used to determine H contents at extremely low concentrations (<1 at. ppm) at micron-scale depth resolution across relatively thick diamond sections (~ ≤ 100 μm) [20]. PPS is particularly useful as it can be used to reconstruct the three-dimensional distribution of H across a diamond section to evaluate controls on H incorporation related to morphology, structural deformation and N content.

In general, the methods described above are reasonably accurate down to H contents of ~ < 50 at.ppm [6] and have shown that the distribution of H in individual diamonds may show considerable heterogeneity (*e.g.* zones with a few ppm to 4000 at.ppm H [6]). This appears to be largely controlled by growth morphology, where cuboid diamond, and/or cuboid sectors in mixed-morphology diamond, tend to show relatively higher H contents than octahedral sectors [2,15,21]. It is not clear if the apparent preferential incorporation of H into cuboid sectors is related to a cuboid growth mechanism or simply the medium from which cuboid growth occurs. However, it has been demonstrated for asteriated diamonds that lobe-shaped, H-rich cuboid sectors and the surrounding octahedral host diamond grew simultaneously [2,22] suggesting that a H-rich growth medium drives the formation of such cuboid sectors due to an increased ability to incorporate H compared to octahedral sectors. Fibrous diamonds (fully fibrous and/or coats, see *e.g.*, [23]) also show relatively higher total H-content than octahedral diamond. However, meaningful comparisons between growth mechanisms are difficult as much of the H in fibrous diamonds is associated with micro- to nano-scale fluid and/or mineral inclusions that may be representative of the diamond forming fluids/melts.

The surface and/or bulk techniques described above do not provide information about the local bonding environment of H in diamond. Therefore, spectroscopic techniques, such as Fourier-transform infrared (FTIR), Raman and ultraviolet-visible (UV–Vis) spectroscopy are used when attempting to understand aspects of H-bonding and H-related defect configurations in diamond. Bulk techniques typically yield total H contents that show poor correlation with H-related peak intensities, the most common of which is the 3107 cm^{-1} peak observed in the FTIR spectra of many *Type Ia* natural diamonds (diamonds that contain N contents detectable by routine FTIR spectroscopy, see Appendix C) which has been attributed to a C-H stretching mode associated with the VN_3H defect (see Section 3.1) [24,25]. Rigorous calculation of H-content by analysis of H-related peaks in the FTIR spectra of diamond is not yet possible as this requires knowledge of exactly which absorption bands involve H and the absorption coefficients of the corresponding H-defects, which may be significantly different for different H-related defects (*e.g.*, [9]). In other words, there is not a 1:1 correspondence between the relative concentration of two different H-defects and the intensity of their signals in the infrared. Moreover, only a small proportion of H in diamond may be (FTIR-) optically-active [6]. Hydrogen may occupy positions associated with defects or lattice interstices where H-bonding has a null (or negligible) dipole moment and is thus optically-inactive. To complicate matters more, significant quantities of optically-active H may be present in micro- to nano-scale fluid and/or mineral inclusions and may correspond to H-related peaks that are incorrectly attributed to discrete $V_xN_yH_z$ defects. Therefore, caution must be taken when evaluating H-related defect concentrations by comparison of FTIR peak intensities, or in general, when attempting to quantify any aspect of H in diamond based solely on peaks intensity (*i.e.*, peak height or area) attributed to H. Nevertheless, several studies have proposed quantitative correlations between total H-content and the intensity of the H-related peak at 3107 cm^{-1} or the calculated concentration of the corresponding VN_3H defect (*e.g.* [6,9,16,26]).

As discussed above, the concentration of H in diamond may vary considerably both within and between different diamonds. With respect to FTIR spectroscopic analysis, H is often detectable in *Type Ia* and occasionally reported in *Type Ib* diamonds (*e.g.*, [27]). Although rare, H has also been detected in *Type IIa* diamonds [7,28] but at relatively low concentrations. To the author's knowledge, H has not been detected in pure *Type IIb* diamonds (*Type IIa/b* diamonds do not contain detectable amounts of N but *Type IIb* diamonds contain B, see Appendix C). It follows that the formation of H-related defects must be largely dependent on N, or more specifically the presence of N- and VN-related defects. Although the kinetic processes associated with the formation of H-related defects are not completely understood, they almost certainly act to inhibit N-aggregation by (1) passivation of dangling C-bonds associated with N- and VN-related defects by interstitial H atoms and/or (2) combination of VN-related defects and other H-related defects [2,9,24,29–33]. There are a large number of possible H-related ($V_xN_yH_z$) defects (see *e.g.*, [34]) and as the majority of diamonds show only a handful of H-related peaks, it is apparent that some defects are more energetically favorable than others. In recent years, first-principles (quantum-mechanical) simulations (*e.g.* [25,35,36]) of FTIR spectra for different H-related defects have aided in the assignment of particular H-related peaks to specific defects (*e.g.,* the 3107 cm^{-1} peak to VN_3H, [24]). Moreover, the discovery and description of a sub-group of natural diamonds termed *hydrogen-rich diamonds* [37,38] have led to the discovery of a large number of H-related peaks that are absent (or have intensities below detection) in most *Type Ia and Type Ib* H-bearing diamonds (*e.g.* [27,29,39–41]. *Hydrogen-rich Type Ia* diamonds are defined by a 3107 cm^{-1} peak intensity greater than the 2158 cm^{-1} peak intensity due to intrinsic lattice vibrations in the two-phonon region [2]. *Hydrogen-rich Type Ib* diamonds on the other hand, are characterized by a relatively larger number of H-related peaks, the strongest of which is typically located at 2972-2973 cm^{-1} [41].

There has been a large amount of work over the last 40 years documenting and interpreting H-related peaks in the FTIR spectra of natural diamond, notable examples include [2,29,30,37,42–44]. However, the most comprehensive of such studies was published over a decade ago (Dischler, [45]) and the growing relevance of diamond (and related materials) in different scientific fields has resulted in a wealth of spectroscopic data dispersed amongst physics, chemistry, geology, mineralogy and crystallography journals. Consequently, interpretation of the poorly understood (*e.g.* H-related) peaks in FTIR spectra of diamond is difficult and often inconsistent due to difficulties relating to interdisciplinary access to related studies. In an attempt to remedy this issue, an updated database of observed and calculated H-related peaks in the FTIR spectra of natural diamonds, compiled from >60 studies from a range of

scientific disciplines, is presented in an attempt to (1) provide a comprehensive framework upon which the assignment and interpretation of H-related peaks can be made, (2) compare calculated and observed peak positions to determine if/why particular $V_xN_yH_z$ defects do not occur in natural diamond and, (3) interpret trends in the occurrence and intensity of H-related peaks as a function of N-aggregation state.

2. An updated FTIR database for H-related peaks

The database was constructed in two parts; (1) observed H-related peaks (Table A.1, Appendix A) and (2) calculated H-related peaks (Tables B.1-B.3, Appendix B). The database focuses solely on the near- and middle-infrared spectra of natural diamond and peaks associated with *X*-H stretching and bending frequencies where X = N, C and B. The methods by which data were processed and organized in the database is described in the following sections. To make this work as accessible as possible to researchers in all disciplines, an introductory section has been included in Appendix C to familiarize the reader with the *Type Classification* of diamond, N-related defects and basic N-aggregation sequences. Following many of the studies included in this paper, a modified nomenclature is used for diamond Type Classification to group data, this is also described in Appendix C.

2.1. Experimental data: Observed H-related peaks

The new database (Table A.1) contains >300 observed peaks attributed to hydrogen impurities in natural diamond. Most H-related peak positions are compiled from numerous studies ([1]-[48], Table A.1), where most peaks are observed in *hydrogen-rich Type Ia* and *Type Ib* diamonds. An additional 60 FTIR spectra of H-bearing, *Type IaB* diamonds were supplied by the *Gemological Institute of America* (GIA, New York) and analyzed by the authors. From these spectra, three *hydrogen-rich* diamonds (samples *G1*, *G2*, and *G3*) were identified and 12 new H-related peaks are reported that, prior to this study, have not been documented in the literature. The vast majority of peaks in Table A.1 are *assumed* to be due to *X*-H vibrational modes as they are not observed in other H-free diamonds and/or because correlations are observed between the intensity of such peaks with other well-characterized H-related peaks (*e.g.* 3107 cm^{-1}) (see *e.g.,* [9,39,45]). Although these assumptions are generally reasonable, one cannot rule out the possibility that some peaks in Table A.1 may be due to vibrational modes associated with other impurities observed in natural diamond such as Ni and Si [45]. However, these impurities are typically observed at low concentrations in natural diamond [46,47] or correspond to absorption frequencies that do not overlap with those related to H (*e.g.* [48,49]). Moreover, no characteristic peaks associated with B-related defects are observed (*e.g.,* 1290, 2460, 2802, 2936 cm^{-1}, [45]). Therefore, it is unlikely that peaks associated with such impurities are incorrectly assigned to H-related peaks in the spectral data included in Table A.1.

In Table A.1, peak positions are listed in order of increasing absorption frequency (wavenumber, cm^{-1}). Additional information (if known) regarding defect-type, stretching/bending modes, normalized peak intensity, diamond type and color and the corresponding references are included for each peak position. Where appropriate, additional comments about the relationship between different peaks (*e.g.,* overtone and combination bands) and/or peak shape (*e.g.,* broad bands, doublet- and shouldered-peaks) is provided. In order to relate different peaks to potential H-related defects, calculated peak positions (and associated defect types, see Section 2.2) within ±2 cm^{-1} of the corresponding observed peak position are also listed. A detailed description of each data category (column) is given in the footnote of Table A.1.

2.1.1. FTIR analyses of hydrogen-rich Type IaB diamonds

FTIR spectra were recorded from samples *G1*, *G2*, and *G3* at the GIA using a Thermo Fisher Nicolet iS50 unit equipped with a KBr beam splitter and a LN-cooled MCT detector. The spectra were recorded at an operating resolution of 1 cm^{-1} with 32 scans, over the range 6000–650 cm^{-1}. These spectra were recorded from cut and polished (round brilliant) diamonds, so thickness corrections cannot be accurately made. Baseline (rubber band) corrections were done using the Fityk V0.9.8 spectra software [50] and H-related peak centers were determined by fitting peaks using pseudo-Voigt functions. The high-frequency range from 6000 to 4600 cm^{-1} of the spectra for samples *G1* and *G3* was cut and removed from each spectrum as no signal was observed in this range.

The full spectra of samples *G1*, *G2*, and *G3* are shown in Figs. 1a, 2a and 3a, respectively. The spectrum of each sample in the one-phonon range from 1550 to 1300 cm^{-1} is shown in Figs. 1b, 2b and 3b to highlight peaks associated with *X*-H bending modes. The spectrum of each sample in the range ~4600 to ~2700 cm^{-1} is shown in Figs. 1c, 2c and 3c to highlight peaks associated with *X*-H stretching modes and overtone and combination bands. In Figs. 1c, 2c and 3c, insets of each spectrum are provided to show the position of several weak peaks near the 3107 cm^{-1} peak and an additional inset in Fig. 2a is included to show the 4704 cm^{-1} and 5888 cm^{-1} combination bands which are only observed in sample *G2*. The intensity of the 3107 cm^{-1} peak in all three samples is greater than the 2158 cm^{-1} peak in the two-phonon region and thus all samples can be classified as *hydrogen-rich* as described in Section 1. Eleven peaks observed at 1398 cm^{-1}, 2723 cm^{-1}, 3035 cm^{-1}, 3076 cm^{-1}, 4442 cm^{-1}, (samples *G1*, *G2*, and *G3*); 4482 cm^{-1} (sample *G2*); 3031 cm^{-1}, 3127 cm^{-1} (sample *G3*); 3090 cm^{-1} (sample *G1*); and 3091 cm^{-1}, 3119 cm^{-1} (samples *G2* and *G3*) have not been documented in the relevant literature until now. However, in many cases these peaks are within 1-3 cm^{-1} from documented peak positions and may represent the same band. Small differences in absorption frequency for the same band may be due to ^{13}C isotopic substitution (*e.g.* [42]), differences in instrumental calibration and/or may be the result of using different methods for the determination of peak position (*e.g.,* peak fitting algorithms).

2.2. Quantum chemical data: First-principles simulations of H-related defects

The continued development of quantum chemical *ab-initio* software programs (*e.g. Crystal23*, [51,52]; *AIMPRO*; *Quantum ESPRESSO* [53,54]; and *ABINIT*, [55]) has prompted much recent work on computing the properties of defects in diamond using Hartree-Fock (HF), Density-Functional Theoretic (DFT) and Molecular Mechanical methods. In several of such studies ([1]-[15], Table B.1) the absorption frequency (cm^{-1}) and intensity of peaks corresponding to vibrational modes for different $V_xN_yH_z$ defects are calculated. This data is compiled in Tables B.1, B.2, and B.3 where peak positions are listed in order of increasing absorption frequency (wavenumber, cm^{-1}) (Table B.1), organized by defect type (Table B.2), and listed in order of increasing absorption frequency for the VN_3H defect (Table B.3). In Tables B.1-B.3, details associated with each peak position are provided and include defect-type, stretching/bending modes, and normalized (to 3107 cm^{-1}) peak intensities. In addition, software and parameters used for each calculation are also provided for each peak position, including defect charge-state, quantum spin-state (S), functionals, cell size (*e.g.,* number of C atoms), basis set, and sampling scheme. Perhaps most importantly, indication of whether or not computation was performed at the *harmonic* or *anharmonic* level is also reported. Tables B.1 and B.2 contain ~315 different peaks that correspond to C-H stretching and bending modes of 14 distinct defects. These include H_1 (and D_1) and H_2 (and H_1D_1), VH_y (y = 1-4), NH_y (y = 1) and VN_xH_y (x = 1-4, y = 1-3) (Table B.2) with variable charge- and spin-states. However, many peaks have null or negligible calculated intensity (normalized to the intensity of the 3107 cm^{-1} peak) and thus are unlikely to be observed when analyzing natural samples.

For any given defect, there is a large degree of scatter in peak

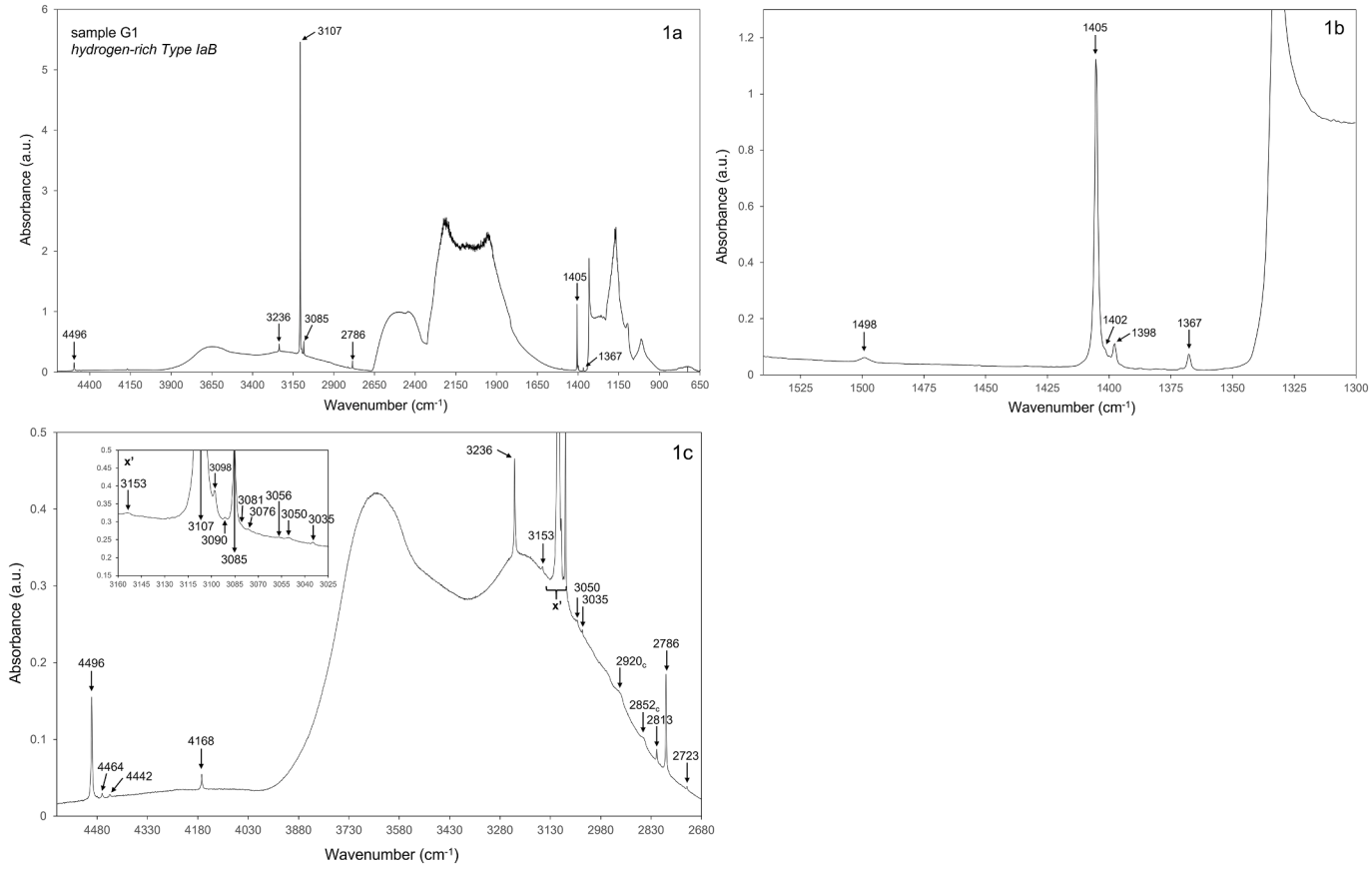

Fig. 1. The FTIR spectrum of a hydrogen-rich Type IaB diamond (Sample *G1*) in the **a)** 4600–650 cm^{-1} frequency range showing several intense H-related peaks, **b)** 1540–1300 cm^{-1} frequency range showing several peaks related to C-H bending modes, and **c)** 4600–2680 cm^{-1} frequency range showing several peaks related to C-H stretching modes and related overtone and combination bands. An additional inset **(x′)** in the 3160–3025 cm^{-1} frequency range is shown to highlight several weak H-related peaks in **c).** Peak positions with a subscripted c (*e.g.* 2920_c) may be due to contamination by grease, glue, or other adhesive materials.

positions (cm^{-1}) as calculations are often performed for variable charge-states and quantum spin-states with different functionals, cell sizes, basis sets and sampling schemes. Calculations are also done using a variety of codes, some of which are not publicly available and thus reproducing simulated spectra is often not possible. Moreover, most of the calculated peak positions do not account for anharmonicity of C-H vibrational modes, which likely has a significant peak-shifting effect for most H-related defects. Duncan et al. [56] and Myrick et al. [57] show that the harmonic-anharmonic shift for the C-H stretching modes of several organic molecules ranges from 100 to 200 cm^{-1}. Salustro et al. [35] show differences in calculated harmonic and anharmonic C-H stretching frequencies for the VH_1 defect (in its doublet and quadruplet spin-state) ranging from 207 cm^{-1} to 335 cm^{-1}. However, these differences are strongly dependent on defect type (and charge-/spin-state) and the functionals used in the computation. For example, Salustro et al. [34] show differences in calculated harmonic and anharmonic C-H stretching frequencies for the VNH_2 (in its doublet spin-state) of 15 cm^{-1} and 35 cm^{-1}, the VNH_3 of 21 cm^{-1} and 57 cm^{-1}, and the VN_2H_2 defect of 1 cm^{-1} and 23 cm^{-1}, respectively. The observed scatter in the calculated peak positions and related issues comparing calculated and observed peak positions are considered more in Section 4.1.

3. $V_xN_yH_z$ defects and associated peaks in the infrared

It is apparent from inspection of Table A.1 that the defect and/or vibrational mode associated with most peaks is unknown. However, several peaks that are relatively common and intense (*e.g.,* 3236 cm^{-1} and 3107 cm^{-1}) have received considerable attention in recent years. In the following section, a brief review of the evidence proposed to support assignment of such peaks to specific H-related defects and/or *X*-H vibrational modes is provided.

3.1. The VN_3H defect and the 3107 cm^{-1} family of peaks

The 3107 cm^{-1} peak was first observed by Charette [58] and is amongst some of the first evidence for H in diamond (*e.g.* [59]). The 3107 cm^{-1} peak is ubiquitous in natural *Type Ia* diamond, is rarely observed as a weak peak in *Type IIa* diamonds [7,28] and is not observed in pure *Type IIb* or *Type Ib* diamonds [41]. The 3107 cm^{-1} band is attributed to a C-H stretching mode based on observation of a bending mode at 1405 cm^{-1} with similar proportional intensity. Additional evidences include an isotopically-shifted ^{13}C band with a position (3098 cm^{-1}) and relative intensity (~1 % of the 3107 cm^{-1} peak, [42]) in accord with the expected ^{12}C-H ➔ ^{13}C-H shifting effect (*e.g.* [60]) and the average ^{13}C content of natural diamond (~1.1 %, [29]).

In diamonds with sufficiently high H contents, additional peaks are observed at higher frequency, with the same proportional intensities relative to the intensity of the 3107 cm^{-1} peak [43]. These peaks correspond to the following overtone and combination bands associated with fundamental C-H stretching (ν_S = 3107 cm^{-1}) and bending (ν_B = 1405 cm^{-1}) modes [37];

2786 cm^{-1} = 2 × ν_B, *overtone.*
4167 cm^{-1} = 3 × ν_B, *overtone.*
4496 cm^{-1} = (1 × ν_B) + (1 × ν_S) *combination.*
5555 cm^{-1} = 4 × ν_B, *overtone.*
5880 cm^{-1} = (2 × ν_B) + (1 × ν_S) *combination.*
6070 cm^{-1} = 2 × ν_S, *overtone.*
8992 cm^{-1} = (2 × ν_B) + (2 × ν_S) *combination.*

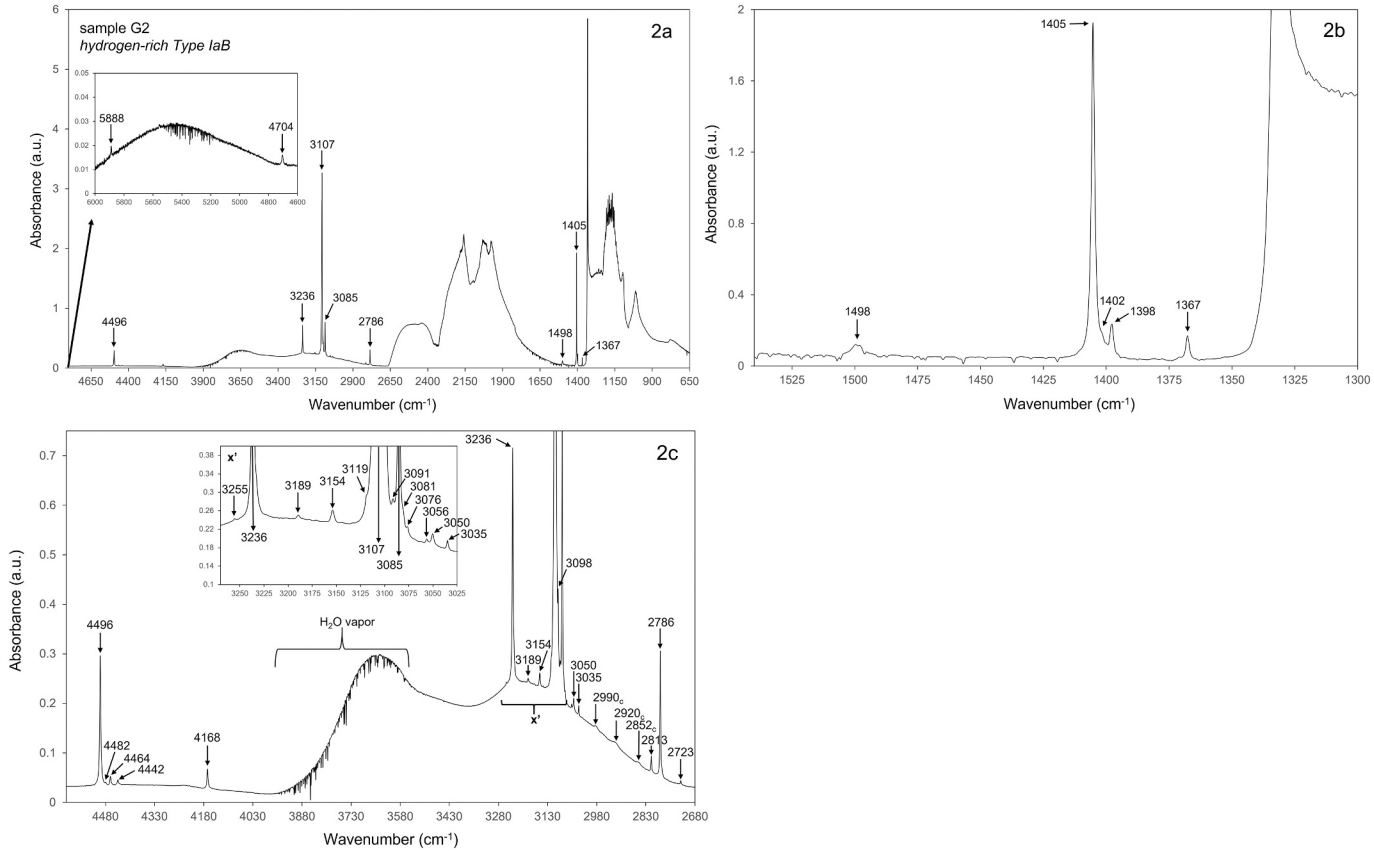

Fig. 2. The FTIR spectrum of a hydrogen-rich Type IaB diamond (Sample *G2*) in the **a)** 4800–650 cm^{-1} frequency range showing several intense H-related peaks. An additional inset in the 6000–4600 cm^{-1} range highlights the 5888 cm^{-1} and 4704 cm^{-1} combination bands. **b)** 1540–1300 cm^{-1} frequency range showing several peaks related to C-H bending modes, and **c)** 4600–2680 cm^{-1} frequency range showing several peaks related to C-H stretching modes and related overtone and combination bands. An additional inset **(x′)** in the 3270–3025 cm^{-1} frequency range is shown to highlight several weak H-related peaks in **c)**. Noise in the 3900–3560 cm^{-1} (in **a)** and **c)**) and 1750–1450 cm^{-1} (in **a)** and **b)**) frequency ranges is due to contamination from atmospheric H_2O vapor. Peak positions with a subscripted c (*e.g.* 2920_c) may be due to contamination by grease, glue, or other adhesive materials.

Many of these peaks are observed in Figs. 1-3 and small discrepancies from the exact overtone and combination products are likely due to anharmonicity associated with ν_S *and* ν_B [43] (see Section 4.1 for discussion about anharmonicity).

Other than the overtone and combination bands, no other peaks have intensities that correlate with the intensity of the 3107 cm^{-1} and/or 1405 cm^{-1} peaks, thus one can assume the associated defect contains one H atom which is related to a single C-H stretching and bending frequency. As shown above, N does not bond to H (or H-bonded C) in this defect. However, the intensity of the 3107 cm^{-1} peak often shows a positive correlation with N content [42,61] and thus one can also assume N is involved in this defect. Moreover, the absence of the 3107 cm^{-1} peak in pure *Type Ib* diamonds suggest involvement of highly aggregated N (*e.g.* N3-centers, VN_3 defects) or B-centers (VN_4 defects) as opposed to C-centers (single substitutional N defects), see Appendix C) and relatively high defect-formation temperatures or long mantle residence times. This is evidenced by several HPHT experiments in which annealing of synthetic *Type Ib* diamond produces a 3107 cm^{-1} peak at 1900-2100 °C where peak intensity increases with increasing temperature up to 2650 °C [61,62]. The 3107 cm^{-1} peak is also observed in CVD diamond during annealing at 2200 °C [63]. Uniaxial stress experiments suggest the defect associated with the 3107 cm^{-1} peak is trigonal and the C-H bond is oriented parallel to the [111] crystallographic axis [64]. Using the evidence described above, Goss et al. [24] assigned the VN_3H defect to the 3107 cm^{-1} peak family as this is the only trigonal defect that involves N and has a single H atom (a single fundamental C-H stretching mode). The VN_3H defect consists of three substitutional N atoms surrounding a vacancy, in which H forms a C-H bond to passivate dangling bonds (uncoupled electrons) of the fourth C atom.

Goss et al. [24] also show that the calculated and observed C-H stretching and bending modes are in good agreement (within 3 %) and suggest the VN_3H defect may form by the trapping of H atoms by N3-centers. This is supported by several studies in which inverse correlations between the intensity of the N3 and 3107 cm^{-1} peaks are observed [9,32]. This formation mechanism would presumably suppress N-aggregation, specifically the transformation of N3- to B-centers and two studies have shown that the concentration of B-centers is inversely correlated with the 3107 cm^{-1} peak area [31,65]. In Fig. 4, different N-aggregation sequences that may produce B-centers and A-centers are shown with solid black lines and two distinct aggregation sequences that may produce N3-centers and thus VN_3H defects are also shown. In Fig. 4, the traditional C → A → B aggregation sequence is shown with colored arrows and, where possible, the defects involved in each aggregation sequence (shown with yellow and white boxes) are plotted with respect to these colored arrows following the results of annealing and spectroscopic studies (as described above). For example, N3-centers are often observed in diamonds with detectable amounts of C-, A- and B-centers and thus it is not required that all (or most) C-centers must aggregate to A-centers before N3-centers can form. Therefore, the VN_3 defects (N3-centers) are shown with white boxes that overlap with the green (C-center), blue (A-center), and orange (B-center) arrows in Fig. 4.

Evidence exists for numerous potential aggregation (or disaggregation) sequences that lead to the production of N3-centers and thus VN_3H defects. Most of these involve different combinations of C- and A-centers or the disaggregation of B-centers due to plastic deformation [66,67] or periods of high-temperature annealing [68] associated with thermal

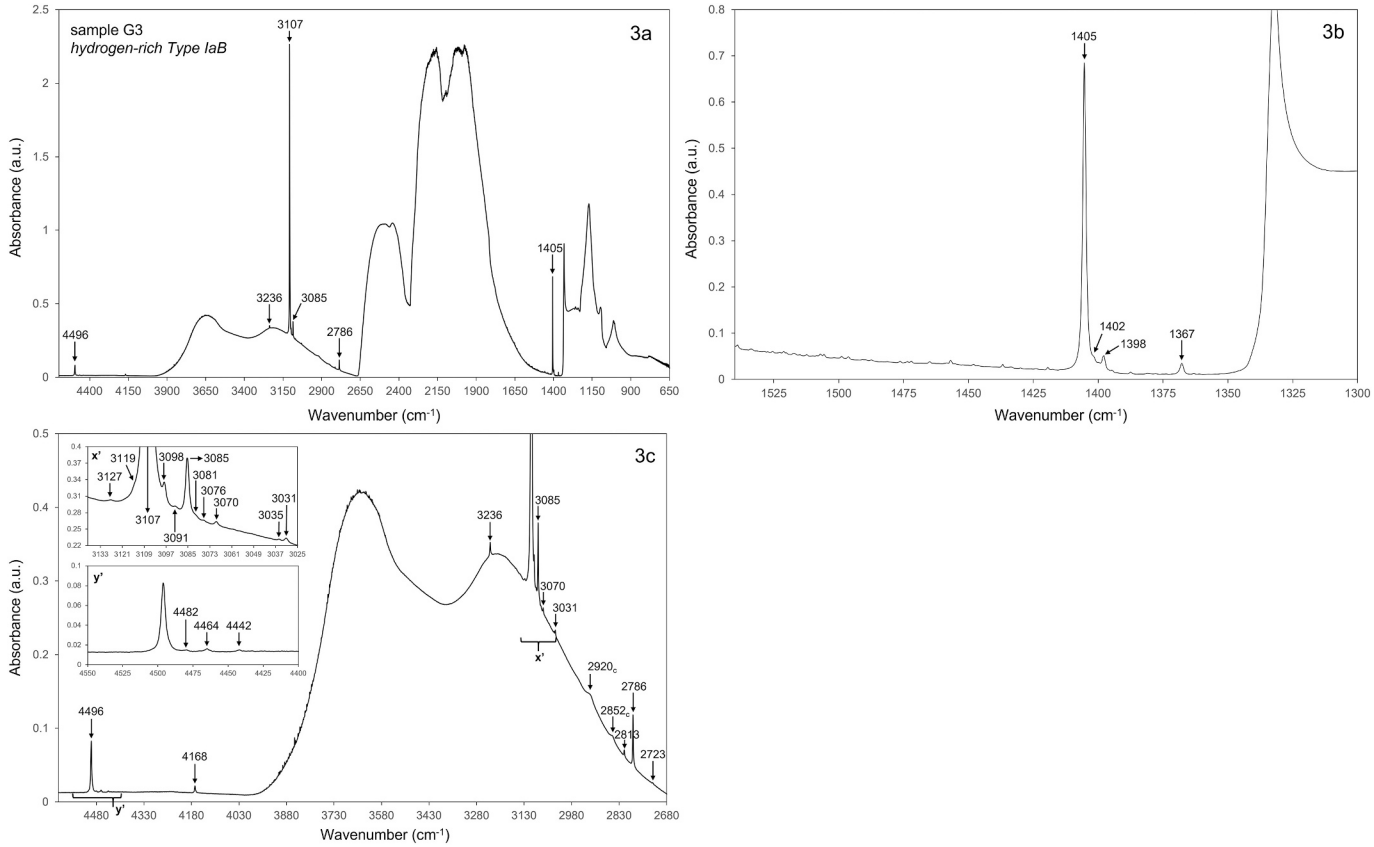

Fig. 3. The FTIR spectrum of a hydrogen-rich Type IaB diamond (Sample *G3*) in the **a)** 4600–650 cm^{-1} frequency range showing several intense H-related peaks, **b)** 1540–1300 cm^{-1} frequency range showing several peaks related to C-H bending modes, and **c)** 4600–2680 cm^{-1} frequency range showing several peaks related to C-H stretching modes and related overtone and combination bands. Additional insets in the 3140–3025 cm^{-1} **(x′)** and 4550–4400 cm^{-1} **(y′)** frequency ranges are shown to highlight several weak H-related peaks due to *X*-H stretching modes and overtones and combinations, respectively. Peak positions with a subscripted c (*e.g.* 2920_c) may be due to contamination by grease, glue, or other adhesive materials.

pulses. An example of B-center disaggregation to produce N3- and C-centers is shown with solid red arrows in Fig. 4, where these N3-centers may eventually trap H to produce VN_3H defects. However, more work is required to reliably link evidence of deformation or HT annealing with evidence for defect disaggregation. Nevertheless, it is possible that some proportion of poorly aggregated N-defects (*e.g.* C-centers) in some diamonds are incorrectly interpreted as primary defects. Such diamonds will inevitably be incorrectly classified and assigned erroneously low mantle residence times and/or temperatures. Woods [69] suggests N3-centers form as a bi-product of the aggregation of A-centers to form B-centers and Kiflawi and Bruley [70] suggest that A-centers must first disaggregate to form isolated N (shown with red dashed arrow, Fig. 4) which later re-combines with A-centers to form N3-centers and interstitial C (C_i). However, annealing studies of natural *Type Ib* diamonds show production of the 3107 cm^{-1} peak coincident with the formation of A-centers and continued increase in the intensity of the 3107 cm^{-1} peak as the concentration of A-centers increases and the concentration of C-centers decreases (*e.g.* [71]). This suggests N3-centers may not be a prerequisite for the formation of VN_3H defects and that several distinct aggregation sequences that produce this defect may be operative in natural diamond. The most common H-related defect in CVD diamond, VNH, (see Section 3.3) has been proposed to form VN_3H defects by combination with A-centers [24,72]. The observation of the *V*NH – C-H stretching mode at 3122-3124 cm^{-1} in *hydrogen-rich* natural diamond [2,21,27] (Table A.1) suggests VN_3H defects may also form by combination of VNH and N_2 defects before the formation of N3- or B-centers in any significant concentration [72]. An example of this aggregation sequence is shown with medium dashed black lines in Fig. 4, where a C-center combines with a vacancy to produce a VN defect that traps H to produce a VNH defect, which in turn combines with an A-center to produce a *V*N_3H defect. H3- and H2-centers (VN_2 in the neutral and negative charge state, respectively) are typically only observed in significant quantities after HPHT treatment of *Type Ia* natural diamonds resulting in the migration of V (in the neutral or negative charge state) and subsequent trapping by A-centers [72,73]. However, a relatively intense H3 peak (503 nm zero-phonon line) in the photoluminescence spectrum of natural *Type IbXY* diamond has been observed [40]. It is possible that, when at significant concentrations, H3-centers may combine with C-centers to produce N3-centers and thus VN_3H defects, this aggregation sequence is shown with short dashed black lines in Fig. 4. The VN_3H defect may also be produced by the combination of a V and a C-center to produce VN which then combines with an A-center to produce a VN_3 defect capable of capturing H, this aggregation sequence is shown with long dashed black lines in Fig. 4. In fact, there are many other aggregation sequences that may form VN_3H defects that are not shown in Fig. 4. However, determining the degree to which these sequences are operative in the early stages of diamond residence requires more work on determining the activation energy of every step in each aggregation sequence (*e.g.* [74–76]).

3.2. The 3236 cm^{-1} peak

The peak observed at 3236-3237 cm^{-1} is commonly observed in *Type Ia* diamonds and is particularly intense in *Type IaB* diamonds. The intensity of the 3236 cm^{-1} peak correlates well with the peaks at 1470 cm^{-1} and 4703-4704 cm^{-1} [37,39] and comprise the system $\nu_S = 3236$ cm^{-1}, $\nu_B = 1470$ cm^{-1} and $\nu_S + \nu_B$ (*combination*) = 4706 cm^{-1}. Unlike the 3107 cm^{-1} peak, only weak correlation between the presence or

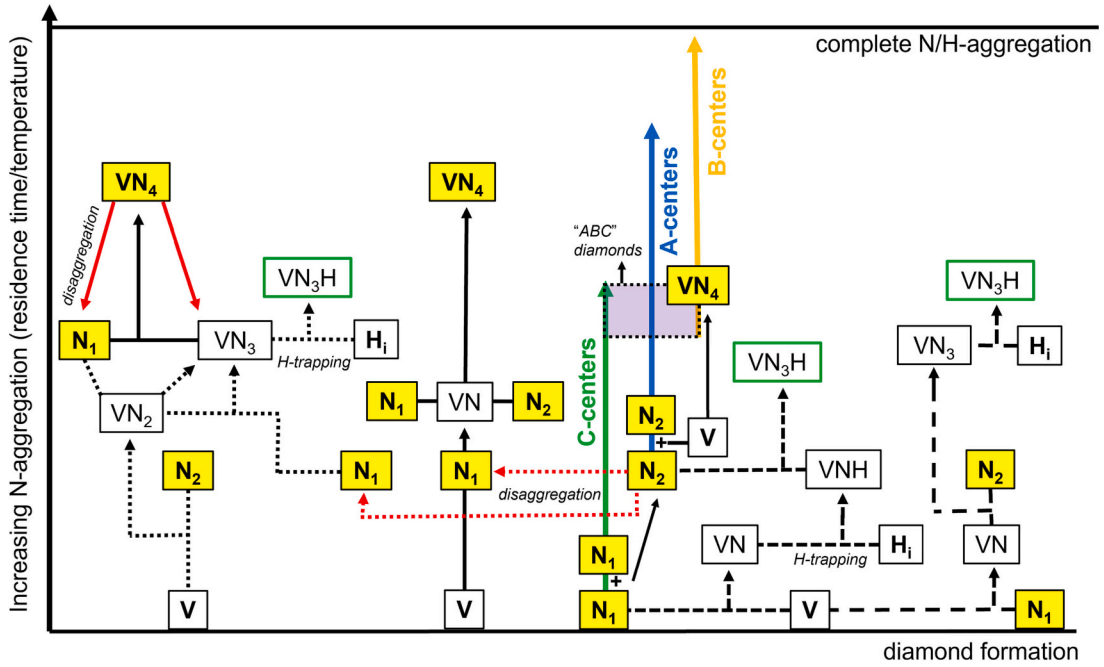

Fig. 4. A flow chart showing different aggregation sequences that may produce the *V*N_3H defect (shown in green boxes) and associated defects such as N3- and B-centers. Aggregation sequences involve the traditional N-related defects, C- (N_1), A- (N_2), and B-centers (VN_4) (shown in yellow boxes) and other defects such as interstitial hydrogen (H_i), singular vacancies (*V*), VN, VN_2, VNH, and VN_3 (shown in white boxes). Simplified aggregation sequences that produce A- and B-centers are shown with solid black lines. Two aggregation sequences that produce VN_3H *via* trapping of H by VN_3 (N3-centers) are shown. In the first, a V and a C-center combine to produce VN which then combines with an A-center to produce VN_3, this aggregation sequence is shown with long dashed black lines. In the second, a V and a A-center combine to produce VN_2 which then combines with a C-center to produce a VN_3 defect, this aggregation sequence is shown with short dashed black lines. Here, the A- and C-centers required to form N3- and B-centers are likely largely primary but may also be produced by the disaggregation of B-centers (solid red lines) or A-centers (dashed red lines). The aggregation sequence that involves trapping of H by VN to produce VNH which in turn, combine with A-centers to produce VN_3H is shown with medium dashed black lines. Based on the results of several annealing/spectroscopic experiments (see Section 3.1), the position of the products (yellow and white boxes) of each step in every aggregation sequence is plotted with respect to the traditional N-aggregation sequences that produce C-centers (green arrow), A-centers (blue arrow), and B-centers (orange arrow). Note how there is a region in which all three of these arrows overlap (purple box) representative of diamonds that contain C-, A-, and B-centers (named "*ABC*" diamonds).

intensity of the 3236 cm^{-1} peak and growth morphology (cuboid *vs.* octahedral sectors) is observed. Moreover, no correlation between the intensity of the 3236 cm^{-1} and 3107 cm^{-1} peaks (or any other C-H stretching peaks) is observed [2]. This can be seen, for example, by comparing these two peaks in Figs. 1a, 2a and 3a. This suggests the 3236 cm^{-1} peak is related to a unique H-related defect that forms independent of the traditional N-aggregation sequence associated with formation of the VN_3H defect (Fig. 4). The above observations and the strong correlation between total N content and 3236 cm^{-1} peak intensity [9] suggest a fundamental N-H stretching mode may be responsible for the 3236 cm^{-1} peak [29,60].

Gu et al. [77] assigned the 3236 cm^{-1} peak to a *platelet-centered* VN_4H defect formed by trapping of H by VN_4 defects. However, in VN_4, each substitutional N forms three covalent C-H bonds with adjacent C atoms and a lone pair. Therefore, in VN_4, there are no uncoupled electrons that may form C-H bonds. Gu et al. [77] reconcile this by proposing a formation mechanism where N substitutes for interstitial C in a platelet and sp^2 hybridization of N and C allow for trapping of H by N and the formation of a VN_4H defect in a pseudo-tetrahedral arrangement. In this defect, two of the N atoms have dangling bonds and Gu et al. [77] suggest a *platelet-centered* VN_4H_2 defect may also form. The platelet-centered VN_4H defect is expected to have only one fundamental stretching and bending mode (one H atom) as is observed for the 3236 cm^{-1} peak. The general negative correlation between the intensities of the 3236 cm^{-1} peak and platelet peak (*e.g.* the 1367 cm^{-1} peak in Figs. 1-3) suggest formation of the VN_4H defect may act to quench platelet growth. In addition, the computed peak positions for the VN_4H defect are in good agreement with the 3236 cm^{-1} peak (see [77]). However, poor correlation between the intensity of the 3236 cm^{-1} peak and the concentration of A-centers and B-centers [9] is problematic. Either there is sufficient H to convert enough B-centers to VN_4H defects such that any correlation is eliminated (or masked) or the aggregation processes responsible for the production of interstitial C and platelets, and thus *platelet-centered* VN_4H defects, occur earlier on (during residence) than traditional C➔A➔B-center sequences (*e.g.* combination of VN_2 and N_2 (A-center)). This may explain the appearance of the 3236 cm^{-1} peak in diamond with a low N-aggregation state.

3.3. Other H-related peaks and associated defects

Song et al. [71] describes a peak at 3143 cm^{-1} in natural *Type Ib* diamond, the intensity of which is roughly correlated with the intensity of the 3107 cm^{-1} peak. The 3143 cm^{-1} peak is only observed in natural diamonds that contain C- and A-centers but not diamonds that contain only C-centers [41,42]. HPHT experiments on natural *Type Ib* diamonds show a coincident increase in the intensity of the 3107 cm^{-1} peak and formation of the 3143 cm^{-1} peak during annealing at 2200 °C [71]. In general, the intensity of the 3143 cm^{-1} peak increases as the ratio of C-centers to A-centers decreases but is not observed when all C-centers are converted to more aggregated forms of N. It follows that formation of the 3143 cm^{-1} defect must be related to the C- to A-center aggregation processes, and the corresponding defect is likely more energetically favorable than C-centers but less favorable than A-centers. Song et al. [71] have assigned the 3143 cm^{-1} peak to a C-H stretching mode associated the "VN_3H…C-N" defect, a VN_3H defect connected to a C-center *via* H bonding.

In Table A.1, several peaks have been tentatively assigned to stretching or bending modes based on spectral similarities with

analogous synthetic samples. The VNH^0 defect is well-characterized in CVD diamond and gives rise to a peak at 3123 cm^{-1} [78–81] and this defect has been assigned to peaks observed at 3122-3124 cm^{-1} in natural diamond. The peaks observed at 3050 cm^{-1} and 3056 cm^{-1} form a doublet (see *e.g.* Figs. 1c and 2c) and are often accompanied by a peak at 3150 cm^{-1} and ~ 3154 cm^{-1} [2], which may represent a corresponding doublet. The peaks at 3050 cm^{-1} and 3150 cm^{-1} are attributed to symmetric and asymmetric N-H stretching modes [82]. The peak at 2982 cm^{-1} has been associated with a peak at 3055 cm^{-1} [83] and may also be assigned to a N-H stretching mode if one assumes this peak is the same as the 3056 cm^{-1} peak. Several peaks in Table A.1 have been assigned to general defects (indicated in square brackets) based on similarities with calculated peak positions. However, due to the large degree of scatter for calculated peak positions (see Section 4.1), this was only done for observed peaks in relatively large frequency ranges that correspond to only one or two possible calculated peaks positions (*e.g.* VH and VNH defects, Table A.1).

4. Discussion

4.1. Defect-peak correlation: Insights from first-principles simulations

The frequency ranges for observed H-related peaks and calculated peaks associated with different $V_xN_yH_z$ defects is shown in Fig. 5. Calculated peak positions for $V_xN_yH_z$ defects show a large degree of scatter, >500 cm^{-1} for most defects. As described in Section 2.2, this is expected, at least to some degree, as for a given defect, peak positions are calculated for different vibrational modes using different levels of theory (*e.g.* local density approximation (LDA) or gradient corrected approximation (GGA) *vs.* "hybrid" functionals (B3LYP) up to the Hartree-Fock approach) at both the harmonic and anharmonic levels. In Fig. 5, functionals are indicated by color and all peak positions calculated at the harmonic and anharmonic level are shown with circles and triangles, respectively. The majority of simulations were done using the PBE or B3LYP functionals (see Table B.1) and in general, the B3LYP functional predicts relatively higher frequencies. The B3LYP functional was used in the majority of anharmonic simulations which appears to shift frequencies to relatively higher wavenumbers compared to identical simulations (using the same functional) completed at the harmonic level.

In Fig. 5, defects are listed based on the number of H atoms they contain (1-4). As the number of N atoms involved in each defect increases, there is minimal (or no) shift in the corresponding peak positions confirming that in these defects N does not participate in H-bonding or bonding to the H-bonded C atom. This is in accord with the absence of peak shifting observed in ^{15}N-doped diamonds [61]. As the number of H atoms in each defect (vacancy) increases from 1 to 4, the average peak position is shifted to higher frequencies (Fig. 5). This trend reflects a progressive decrease in the average C-H bond distance due to mutual electrostatic repulsion between H in the vacancy. For VN_xH_y defects (where $x = 1$ to 3, and $y = 1$ to 3), Salustro *et al* [35] show that C-H bond distances decrease from $y = 1$ to 3 for a given value of x. For example, the C-H bond distances reported by [35] for the defects VNH, VNH_2, and VNH_3 are 1.082, 1.052, and 1.034 Å, respectively. However,

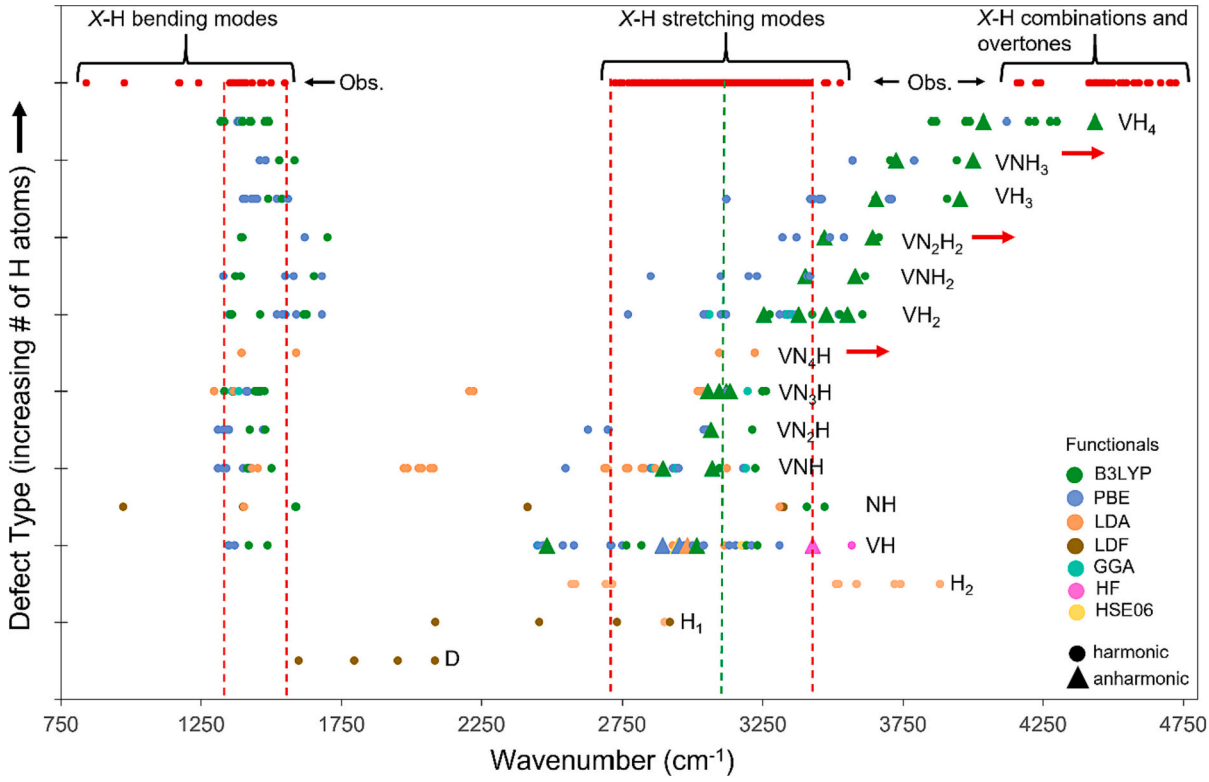

Fig. 5. Observed peak positions corresponding to *X*-H bending and stretching modes shown at the top of the figure with red circles, note that these points form a continuum from 2700 to 3450 cm^{-1}. The calculated peak positions corresponding to *X*-H bending and stretching modes for different $V_xN_yH_z$ defects where x = 0-1, y = 0-4, and z = 0-4 are shown with colored circles and triangles. The observed and calculated peaks corresponding to fundamental *X*-H bending (1350-1550 cm^{-1}) and stretching (2700-3450 cm^{-1}) modes overlap largely for all defects except VH_3, VNH_3 and VH_4 (red dashed vertical lines). The green dashed vertical line indicates the 3107 cm^{-1} peak which overlaps with the calculated peak positions for the C-H stretching mode of the VN_3H defect, specifically those calculated at the anharmonic level. All $V_xN_yH_z$ defects are plotted in order of increasing number of H atoms where defects contain one, two, three, and four H atoms. Here, as the number of H atoms involved in each defect increases, there is a systematic increase in the peak position (cm^{-1}) (shown with red arrows) but no increase in the average peak position as the number of N atoms involved in the defect increases. The type of functional used in each calculation are indicated by color and frequencies calculated at the harmonic and anharmonic levels are shown with circles and triangles respectively.

the degree of repulsion amongst H atoms in a vacancy (and thus the corresponding C-H bond-distances and stretching frequencies) are also controlled by the C-H bond polarity (which can be estimated from the difference in net atomic charge (|e|) of C and H, as evaluated from a Mulliken partition of the charge density function). Salustro et al. [35] shows that for a given VN_xH_y defect, the C-H bond polarity, for a given value of *y*, increases as *x* increases, which in general, acts to increase the mutual repulsion between H atoms and reduce the C-H bond distances. The quantum spin-state of the defect also influences the C-H bond-distance, for example the VNH defect in a singlet and triplet spin-state has C-H bond distances of 1.072 and 1.082 Å, respectively [35].

Inspection of Fig. 5 shows that there is almost complete overlap between observed and calculated peak positions associated with *X*-H bending modes for all defect types. The majority of observed peak positions associated with fundamental *X*-H stretching modes plot in the range 2720-3420 cm^{-1} (red dashed lines, Fig. 5) and overlap almost completely with calculated peak position for all defect types except VH_3, VNH_3 and VH_4. Although it may appear that there is overlap between observed peaks and calculated peaks for the VH_4 defect between 4167 and ~4450 cm^{-1}, these observed peaks correspond to overtone and/or combination bands (*e.g.* see Section 3.1) not fundamental *X*-H stretching modes. The lack of overlap between observed peak positions and those computed for the VH_3, VNH_3 and VH_4 defects is in accord with our current understanding of N/H-aggregation in natural diamond. In general, the intensity of H-related peaks increases with N content and the trapping of H to form $V_xN_yH_z$ defects is driven by production (and subsequent passivation) of dangling carbon bonds through substitution of C for N. As H content in most *Type I* diamonds is relatively low compared to N content, it is unlikely that isolated vacancies (instead of N) serve as the dominant mode of H trapping, especially as such vacancies are a means by which N migrates and aggregates [74,84]. Moreover, the thermal equilibrium concentration of V has been shown to be several orders of magnitude less than the average N concentration in diamond at upper mantle temperatures (<1500 °C) [74]. However, it has also been shown that the concentration of vacancies in octahedral (111) growth sectors may be larger than in cuboid (100) sectors [74], which in turn, may explain why N-aggregation occurs at a faster rate in octahedral sectors compared to cuboid sectors (octahedral sectors have a lower C- > A-center activation energy (E_a)) [76,84]. Regardless of growth morphology, an extremely H-rich and N-poor growth medium would be required for the formation of defects such as VH_3 and VH_4, especially in concentrations sufficiently high to be observed in the infrared.

The computed peak positions for the VN_3H defect show relatively less scatter compared to the other defects and, as expected, overlap with the 3107 cm^{-1} peak position (green dashed line, Fig. 5). Inspection of Table B.3 shows that computed peaks for the C-H bending mode range from 1296 to 1476 cm^{-1} and the 1411 cm^{-1} peak [36] is in closest agreement with the observed VN_3H – C-H bending mode at 1405 cm^{-1} (calculated peaks are within 0.4 to 8 % of 1405 cm^{-1} peak). Computed peaks for the C-H stretching mode range from 3018 to 3262 cm^{-1} and the 3094 and 3120 cm^{-1} peaks [25,85] are in closest agreement with the observed VN_3H – C-H stretching mode at 3107 cm^{-1} (calculated peaks are within 0.4 to 5 % of 3107 cm^{-1} peak). The 3094 cm^{-1} peak position was calculated at the anharmonic level and in general, anharmonic peak positions are in closer agreement with the 3107 cm^{-1} peak (within 0.4 to 1.7 %) (Table B.3).

In several studies, agreement between calculated and observed peak positions is used to confirm peak-defect assignments. For example, Goss et al. [24] produce calculated peak positions for the VN_3H – C-H bending and stretching modes within 3 % of the observed 1405 and 3107 cm^{-1} peaks. Gu et al. [77] produce calculated peak positions of 3095 and 3221 cm^{-1} for the VN_4H – C-H stretching modes within 0.5 to 4 % of the observed 3236 cm^{-1} peak to which they consequently assign to the VN_4H defect. As discussed in Sections 3.1 and 3.2, Goss et al. [24] and Gu et al. [77] use other lines of evidence to support these peak-defect assignments as the degree of scatter for calculated peak positions is large. For example, 3 % of the 3107 cm^{-1} peak is 93 cm^{-1} and inspection of Table A.1 shows many calculated peak positions that plot in this range and that are associated with defects different than VN_3H including VH, VH_2, VH_3, VNH, VN_2H, VN_4H, VNH_2 and VN_2H_2. Moreover, there are six calculated peak positions in closer agreement with the 3107 cm^{-1} peak than the 3094 and 3120 cm^{-1} peaks, these include 3118 cm^{-1} (VH_2^-), 3114 cm^{-1} (VH^0), 3100 cm^{-1} (VH_2^+ and VNH_2^-), 3096 cm^{-1} (VNH) and 3095 cm^{-1} (VN_4H). The case is similar for the 3236 cm^{-1} peak, where there are five calculated peak positions in closer agreement with the 3236 cm^{-1} peak than the calculated 3221 cm^{-1} peak which is used as evidence for assignment of this peak to VN_4H [77]. These peaks include 3250 and 3249 cm^{-1} (VN_3H), 3231 cm^{-1} (VH), 3230 cm^{-1} (VNH_2^0) and 3224 cm_{-1} (VNH).

In general, variability in the computed peak positions for a given vibrational mode of a specific defect is too large to make meaningful assignments of such defects to observed peaks. Moreover, as anharmonicity is not accounted for in the computation of most peak positions (see Tables B.1 and B.2), it is unreasonable to expect them plot in good agreement with the corresponding observed peaks unless one assumes *X*-H vibrational modes in diamond are largely harmonic which is not the case. For vibrational modes that involve heavier atoms (compared to H) the anharmonic contribution to the stretching frequency is typically small and can be ignored or accurately approximated using perturbation theory. However, the anharmonic contribution to *X*-H stretching modes is much larger due to the low atomic mass of H and more rigorous methods are required to correct for anharmonicity. Such corrections have become extremely effective and have seen considerable use in programs like *Crystal23* (*e.g.* the ANHARM correction, [51]). However, as there is a large number of observed H-related peaks within 1-5 cm^{-1} of one another (see Table A.1), quantum mechanical calculations (and associated corrections) must be capable of simulating peaks positions with a similar resolution, and this is not currently the case. It follows that one cannot make definitive peak-defect assignments using *only* calculated peak positions and it is therefore imperative to use additional evidence (*e.g.* defect symmetry, peak intensity correlations, *etc.*) to support peak-defect assignments as was done in the studies by Goss et al. [24] and Gu et al. [77].

4.2. Observed peak positions and N/H-aggregation processes

The spectroscopic study of H-related peaks has drastically improved our understanding of the relative stability and configurations of several $V_xN_yH_z$ defects. However, the mechanisms by which N/H-related defects form and aggregate with increasing residence time and temperature remains poorly understood. Describing any N/H-aggregation process requires that one defines the *initial* and *final* environment (*i.e.,* position and bonding environment) of H and N atoms. In most *Type Ia* diamonds the final (optically-active) environment of H appears to be largely associated with the 3107 cm^{-1} family of peaks (VN_3H), and to a much lesser extent, weaker peaks such as 3236 cm^{-1}. Defining the initial environment of H is much more difficult as the mechanisms by which H is incorporated during natural diamond formation are unknown. Moreover, the degree of post-growth equilibration *via* H diffusion is also largely unknown. However, several studies suggest the diffusion of H is strongly impeded in diamonds that contain various point- (*e.g.* $V_xN_yH_z$ defects) and extended-defects (*e.g.* platelets) [14,17,86]. Most hydrogen-rich *Type Ia* and *Ib* diamonds show elevated N contents compared to low-H *Type Ia* and *Ib* diamonds and in general, the intensity of H-related peaks increases with N content (*e.g.* the 3107 cm^{-1} peak is only observed in diamonds with aggregated N) (see *e.g.*, [31,65,87]). However, no statistically meaningful correlation between measured H and N content has been observed and thus it appears that H and N incorporation during diamond growth is not correlated [15]. It follows that vacancies, N and H are unlikely to be incorporated as aggregate defects during diamond formation and growth and instead, form from

annealing starting in the early stages of residence in the mantle and/or possibly within diamond cores in the later stages of diamond formation. The majority of H may be initially incorporated as atoms/ions interstitial to the diamond lattice but may also be associated with intragrain boundaries, inclusions, and/or dislocations.

In Fig. 6, all observed peak positions are plotted as a function of diamond type (N-aggregation state) from *Type Ib + IbXY* to *Type IaB* and thus define a trend of increasing aggregation state and mantle residence time/temperature. Peaks observed in *Type Ib* diamonds in which X- and Y-centers were not recognized are grouped with peaks observed in *Type Ib + IbXY* diamonds. Most *Type Ib* diamonds (that are not hydrogen-rich) are characterized by only a handful of H-related peaks (*e.g.* 3394, 3372, 3310, 3181, 3145 and 3137 cm^{-1}, see [42,88]). Such peaks likely represent the most abundant (energetically favorable) $V_xN_yH_z$ defects in *Type Ib* diamond or have a relatively large absorption coefficient as *hydrogen-rich Type Ib + IbXY* diamonds show a significantly larger number of H-related peaks (*e.g.,* [27,29,37,40,83,89,90]). As there is no evidence to support coupled incorporation of H and N (as described above), it is likely that these defects form through trapping of interstitial H shortly after diamond formation has occurred.

In *Type IaA + Ib* diamonds, the formation of A-centers (dashed blue line, Fig. 6) coincides with a significant increase in the number of unique peak positions (compared to *Type Ib + IbXY*) which plot over much of the frequency range from 2800 to 3400 cm^{-1} (Fig. 6). In *Type Ib + IbXY* and *Type IaA + Ib* diamonds, peaks associated with the 3107 cm^{-1} family and the 3236 cm^{-1} peak are not observed as these defects are associated with a higher degree of N aggregation. Instead, most peaks in *Type Ib + IbXY* and *Type IaA + Ib* diamonds are likely associated with poorly aggregated $V_xN_yH_z$ defects (*i.e.,* defects involving singular N like NH) and related extended defects that involve numerous H atoms giving rise to multiple C-H and N-H vibrational modes. It is evident that the majority of such defects have a relatively lower stability with increasing mantle residence time/temperature than those in diamonds dominated by A- and B-centers as the majority of peaks in *Type Ib + IbXY* and *IaA + Ib* diamonds are absent in *Type IaA > Ib* diamonds. At this point, where the majority of C-centers in *Type IaA + Ib* diamonds, aggregate to form A-centers in *Type IaA > Ib* diamonds, (red dashed line, Fig. 6) there is a major decrease in the number of distinct H-related peaks. Approximately 51 % of observed H-related peaks are only observed in *Type Ib + IbXY* and *IaA + Ib* diamonds, ~9 % of peaks are only observed in diamonds with a dominant *Type Ia* character and ~40 % of peaks are observed in diamonds with a dominant *Type Ia* character and diamonds with a dominant *Type Ib* character.

Most of the defects associated with the relatively large number of H-related peaks observed in *Type IaA + Ib* diamonds (Fig. 6) aggregate (or disaggregate) to form drastically fewer peaks (and presumably fewer distinct $V_xN_yH_z$ defects) in *Type IaA > Ib* diamonds. Many of these peaks (and the corresponding defects) appear to persist through continued annealing and N-aggregation as they are observed in *Type IaA > B > Ib, IaB > A > Ib, IaA, IaAB, and IaB* diamonds (*e.g.,* 3236 cm^{-1}) (Fig. 6). It follows that there may be a major increase in the stability of defects produced through aggregation sequences associated with the formation of A-centers and loss of C-centers. As described in Section 1, *hydrogen-rich Type Ib* diamonds show a large number of H-related peaks that are significantly less intense than most peaks observed in *Type IaA*, *IaAB* and *IaB* diamonds. If one assumes the majority of H is trapped in the early

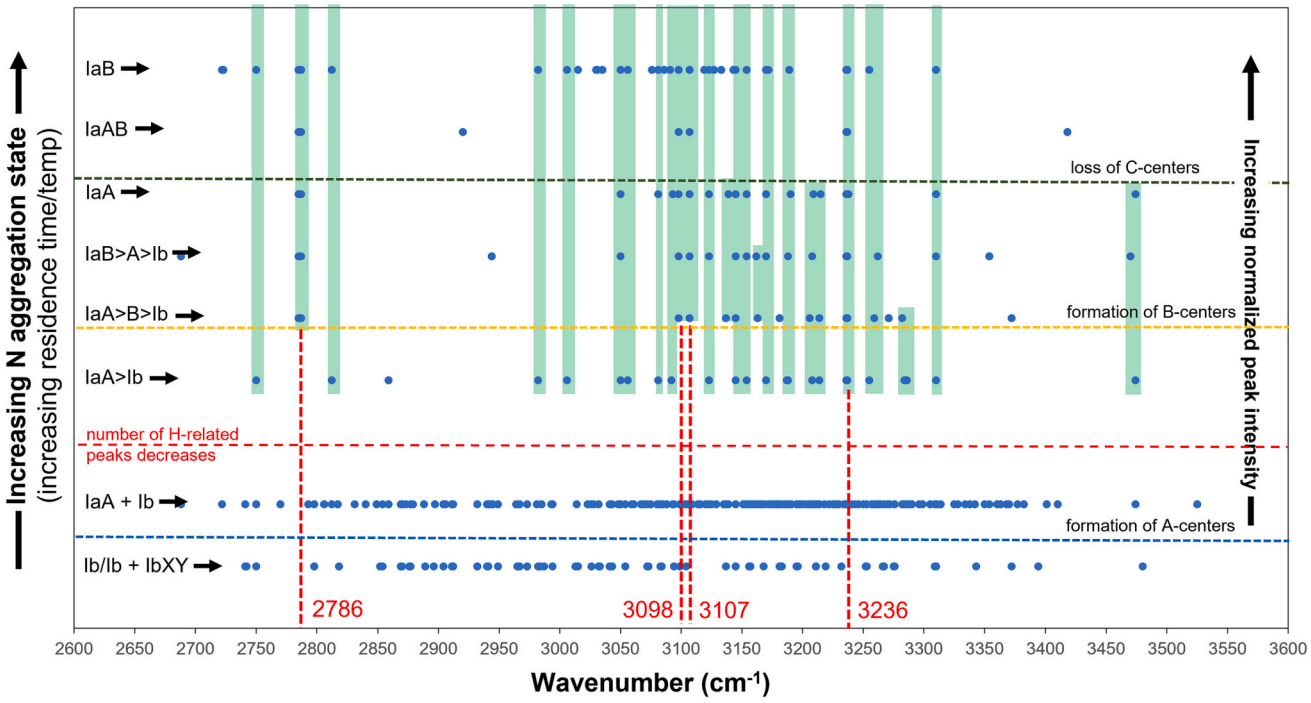

Fig. 6. Hydrogen-related peak positions (shown as blue circles) observed in the frequency range 3600–2600 cm^{-1} plotted as a function of diamond type. Peak positions are plotted in order of increasing N-aggregation state from *Type Ib/Ib + IbXY* to *Type IaB* which reflects a general increase in mantle residence time and/or temperature. An increase in the number of distinct H-related peaks occurs coincident with the formation of A-centers (dashed blue line) from *Type Ib/Ib + IbXY* to *Type IaA + Ib* diamonds. A drastic decrease in the number of distinct peaks occurs coincident with an increase in the proportion of A-centers and a decrease in the proportion of C-centers in *Type IaA > Ib* diamonds (red dashed line). The formation of B-centers in *Type IaA > B > Ib* diamonds marks the appearance of several distinct peaks (orange dashed line) that are not observed in *Type IaA > Ib* diamonds. The complete loss of C-centers in *Type IaA* diamonds (green dashed line) marks the disappearance of peaks that are observed in *Type IaA > Ib*, *Type IaA > B > Ib, Type IaB > A > Ib,* and *Type IaA* diamonds but not in *Type IaAB* and *IaB* diamonds. The formation of the VN_3H defect appears to be associated with aggregation sequences that produce B-centers as the 2786 cm^{-1} and 3107 cm^{-1} peaks are only observed in diamonds with a *Type IaB* component (thick red dashed line). The formation of the defect corresponding to the 3236 cm^{-1} peak appears to be associated with the formation of A-centers as this peak is observed in all diamond types except *Type Ib + IbXY*. Peak positions that are observed in one or more diamonds types are colored green to highlight defects that persist through progressive annealing over varying ranges of N-aggregation from *Type IaA > Ib* to *Type IaB* diamonds.

stages of diamond residence, diffusive loss or gain of H is likely minimal during residence in the mantle. This observation is in accord with the trends observed in Fig. 6. During N-aggregation, H-related defects in *Type Ib + IbXY* and *IaA + Ib* diamonds and other forms of optically-inactive H combine to form fewer defects at relatively higher concentrations that give rise to relatively more intense H-related peaks. Of course, one cannot rule out that the large number of peaks in *Type Ib + IbXY* and *IaA + Ib* diamonds may also be due to the presence of defects with a relatively large number of distinct fundamental *X*-H vibrational modes but this is likely not the case as higher degrees of N/H-aggregation would be required to form defects that contain three and four H atoms and thus more vibrational modes.

There are also several peaks that are only observed in *Type IaB* diamonds such as 2722-2723 cm^{-1}, 3015 cm^{-1}, 3031 cm^{-1}, 3035 cm^{-1}, 3076 cm^{-1}, and 3133 cm^{-1} that must correspond to defects associated with highly aggregated N and that form in the later stages of N-aggregation. The formation of B-centers and *Type IaA > B > Ib* diamonds (dashed orange line, Fig. 6) marks the appearance of several peaks (*e.g.* 2786, 3098, 3107 cm^{-1}) that are likely associated with the formation of B- or N3-centers. With continued N-aggregation and the eventual complete loss of C-centers and formation of *Type IaA* diamonds (dashed green line, Fig. 6), several peaks disappear (*e.g.* 3137, 3139, 3209, 3215 and 3474 cm^{-1}). Inspection of Fig. 6 also shows several peaks that are observed in only specific diamond types such as 3372 cm^{-1} in *Type IaA > B > Ib* diamonds; 2688 cm^{-1}, 2944 cm^{-1} and 3354 cm^{-1} in *Type IaB > A > Ib* diamonds; and 3418 cm^{-1} in *Type IaAB* diamonds. It follows that the corresponding defects must be only temporarily stable and may form as by-products of different N/H-aggregation processes.

5. Conclusions

An updated and comprehensive database of observed H-related peaks along with details regarding associated defects, vibrational modes, diamond types and relative (normalized) peak intensities are provided to facilitate the recognition and comparison of H-related peaks in future work. In addition, a database of computed peak positions for a variety of $V_xN_yH_z$ defects is provided to allow for comparison with observed peaks and to assess the viability of first-principles simulations as a method by which one can make peak-defect assignments. For any given defect, the scatter in calculated peak positions is large. Until more accurate methods for approximating the frequency shifting effect of anharmonicity of C(N)-H bonds are developed, peak-defect assignments based solely on agreement between observed and calculated peak positions should be avoided unless additional evidence (*e.g.* defect symmetry, peak intensity correlations, *etc.*) is provided to support the peak-defect assignment. Moreover, the lack of overlap between observed peaks positions and those calculated for defects such as VH_3, VNH_3 and VH_4 and the general correlation between elevated H and N defect concentrations in natural diamonds, suggests aggregated N is required to effectively trap H. Thus N (in any aggregation state) is likely a pre-requisite for the formation of aggregated H-related defects.

Compilation of a large number of observed H-related peaks for a variety of diamond types (N-aggregation states) allows for several fundamental observations to be made about N/H aggregation processes in natural diamond. With increasing N-aggregation (annealing time/temperature), coupled N/H-aggregation processes act to reduce the number of observed H-related peaks in *Type Ib + IbXY* and *Type IaA + Ib* diamonds through formation of fewer, presumably more stable $V_xN_yH_z$ defects. These defects in *Type IaAB* and *IaB* diamonds correspond to peaks that, on average, are more intense than in *Type Ib + IbXY* and *Type IaA + Ib* diamonds. This suggests that defects associated with higher degrees of N-aggregation form by not only trapping optically-inactive H, but through combination of a large number of different defects (in *Type IaA + Ib* and *Type Ib* diamonds) that become unstable (energetically less favorable) with increasing residence time/temperature in the mantle. This transition point (Fig. 6, red dashed line) appears to be associated with the progressive aggregation of C-centers to A-centers as significantly less (relatively more intense) peaks are observed in diamonds with a dominant *Type IaA* and *IaB* character compared to hydrogen-rich diamonds with a dominant *Type IaA + Ib* and *Type Ib + IbXY* character. It is important to note that the majority of peaks observed in hydrogen-rich *Type Ib + IbXY* diamonds are not observed in *Type Ib* diamonds that are not hydrogen-rich. Thus, it is tempting to assume that the H content of a *Type Ib* diamond may influence the occurrence of different $V_xN_yH_z$ defects. However, this is unlikely as the N (and vacancy) content is much greater than that of H in most natural diamond and the intensity of H-related peaks in typical *Type Ib* diamond (that is not hydrogen-rich, see Section 4.2) does not increase significantly in hydrogen-rich *Type Ib + IbXY* diamonds. Instead, it is likely that the majority of H-related peaks in hydrogen-rich *Type Ib + IbXY* diamonds are below detection in *Type Ib* diamonds that are not hydrogen-rich. However, it remains unclear what proportion of H-related peaks are associated with X- and Y-centers (compared to C-centers) in *Type Ib + IbXY* diamonds.

To conclude, it is clear that future work on assigning H-related peaks to specific defects in diamonds with a dominant *Type Ib*, *IaA* and *IaB* character is needed. This will allow us to better understand the kinetic processes associated with the migration of N and H in diamond, how and in what form N and H are incorporated during growth, and in what sequence $V_xN_yH_z$ defects form during progressive diamond growth and/or during the early stages of residence in the mantle.

Funding

Funded by the European Union (ERC, INHERIT, starting grant no. 101041620). Views and opinions expressed are however those of the author(s) only and do not necessarily reflect those of the European Union or the European Research Council Executive Agency. Neither the European Union nor the granting authority can be held responsible for them.

CRediT authorship contribution statement

Maxwell C. Day: Writing – original draft, Formal analysis, Conceptualization. **Michael C. Jollands:** Writing – review & editing, Resources, Investigation. **Davide Novella:** Writing – review & editing, Visualization, Conceptualization. **Fabrizio Nestola:** Writing – review & editing. **Roberto Dovesi:** Validation, Formal analysis. **Martha G. Pamato:** Writing – review & editing, Supervision, Conceptualization.

Declaration of competing interest

The authors have no financial interests and have no other conflicts of interest to disclose.

The authors confirm that this work is original and has not been published elsewhere, nor is it currently under consideration for publication elsewhere.

Data availability

The data in Table 1 (Appendix A) and Tables 2-4 (Appendix B) and the FTIR spectra of samples G1, G2, and G3 can be accessed from the University of Padova repository at https://researchdata.cab.unipd.it/1184/

Acknowledgements

We thank Mauro Prencipe (University of Torino) for his advice regarding the construction of Tables B.1-B.3 and for the informative discussions about the anharmonicity of O-H and C-H vibrational modes.

Appendices. Supplementary data

Supplementary data to this article can be found online at https://doi.org/10.1016/j.diamond.2024.110866. This supplementary data and the raw data for spectra G1, G2, and G3 can also be found online at the University of Padova repository at https://researchdata.cab.unipd.it/1184/.

References

[1] C.H. Van der Bogert, C.P. Smith, T. Hainschwang, S.F. McClure, Gray-to-blue-to-violet hydrogen-rich diamonds from the Argyle Mine, Australia, Gems Gemol. 45 (2009) 20–37.

[2] B. Rondeau, E. Fritsch, M. Guiraud, J.-P. Chalain, F. Notari, Three historical 'asteriated' hydrogen-rich diamonds: growth history and sector-dependent impurity incorporation, Diam. Relat. Mater. 13 (2004) 1658–1673, https://doi.org/10.1016/j.diamond.2004.02.002.

[3] M.C. Day, M.G. Pamato, D. Novella, F. Nestola, Imperfections in natural diamond: the key to understanding diamond genesis and the mantle., La Rivista Del Nuovo Cimento. In-Press (accepted) (2023) 1–140.

[4] E. Sideras-Haddad, S.H. Connell, J.P.F. Sellschop, I.Z. Machi, D. Rebuli, R. D. Maclear, B.P. Doyle, Hydrogen and oxygen chemistry and dynamics in diamond studied by nuclear microscopic techniques, Nucl. Inst. Methods Phys. Res. B (2001), https://doi.org/10.1016/S0168-583X(01)00595-X.

[5] J.P.F. Sellschop, C.C.P. Madiba, H.J. Annegarn, Light volatiles in diamond: physical interpretation and genetic significance, Nucl. Inst. Methods 168 (1980) 529–534, https://doi.org/10.1016/0029-554X(80)91305-1.

[6] R.J. Sweeney, V.M. Prozesky, K.S. Viljoen, S. Connell, The sensitive determination of H in diamond by infrared (FTIR) spectroscopy and micro-elastic-recoil (μ-ERDA) techniques, Nucl. Inst. Methods Phys. Res. B 158 (1999) 582–587, https://doi.org/10.1016/S0168-583X(99)00367-5.

[7] P.R.W. Hudson, I.S.T. Tsong, Hydrogen impurity in natural gem diamond, J. Mater. Sci. 12 (1977), https://doi.org/10.1007/BF00553924.

[8] V. Rupertus, Ion beam spectrochemical analysis (IBSCA), in: Surface and Thin Film Analysis, Wiley, 2011, pp. 357–366, https://doi.org/10.1002/9783527636921.ch22.

[9] J.O. Wood, An Elusive Impurity: Studying Hydrogen in Natural Diamonds, University of Bristol, 2020.

[10] H. Bureau, C. Raepsaet, H. Khodja, A. Carraro, C. Aubaud, Determination of hydrogen content in geological samples using elastic recoil detection analysis (ERDA), Geochim. Cosmochim. Acta 73 (2009) 3311–3322, https://doi.org/10.1016/j.gca.2009.03.009.

[11] B.P. Doyle, R.D. Maclear, S.H. Connell, P. Formenti, I.Z. Machi, J.E. Butler, P. Schaaff, J.P.F. Sellschop, E. Sideras-Haddad, K. Bharuth-Ram, 3-D-micro-ERDA microscopy of trace hydrogen distributions in diamond using a 2-D-PSD with event reconstruction, Nucl. Inst. Methods Phys. Res. B 130 (1997) 204–210, https://doi.org/10.1016/S0168-583X(97)00367-4.

[12] S.H. Connell, J.P.F. Sellschop, J.E. Butler, R.D. Maclear, B.P. Doyle, I.Z. Machi, A study of the mobility and trapping of minor hydrogen concentrations in diamond in three dimensions using quantitative ERDA microscopy, Diam. Relat. Mater. 7 (1998) 1714–1718, https://doi.org/10.1016/S0925-9635(98)00266-0.

[13] R.D. Maclear, S.H. Connell, B.P. Doyle, I.Z. Machi, J.E. Butler, J.P.F. Sellschop, S. R. Naidoo, E. Fritsch, Quantitative trace hydrogen distributions in natural diamond using 3D-micro-ERDA microscopy, Nucl. Inst. Methods Phys. Res. B 136–138 (1998) 579–582, https://doi.org/10.1016/S0168-583X(97)00701-5.

[14] A.A. Shiryaev, D. Grambole, A. Rivera, F. Herrmann, On the interaction of molecular hydrogen with diamonds: an experimental study using nuclear probes and thermal desorption, Diam. Relat. Mater. 16 (2007) 1479–1485, https://doi.org/10.1016/j.diamond.2006.12.005.

[15] D. Vangu, H. Bureau, H. Khodja, M. Charrondiere, I. Esteve, K. Béneut, L. Remusat, E. Gaillou, P. Cartigny, J.-C. Bouillard, Combination of ERDA, FTIR spectroscopy and NanoSIMS for the characterization of hydrogen incorporation in natural diamonds, Diam. Relat. Mater. 136 (2023) 110007, https://doi.org/10.1016/j.diamond.2023.110007.

[16] V.F. Kaminsky, Ya.B. Ber, Yu.D. Kazantsev, K.G. Khachatryan, N.S. Shilobreeva, Hydrogen in natural diamond: comparison of SIMS and FTIR data, Research Square (Preprint). (2020) 1–17.

[17] F. Jomard, D. Ballutaud, SIMS analysis of hydrogen diffusion and trapping in CVD polycrystalline diamond, Appl. Surf. Sci. 203–204 (2003) 478–481, https://doi.org/10.1016/S0169-4332(02)00745-6.

[18] F.A. Stevie, C. Zhou, M. Hopstaken, M. Saccomanno, Z. Zhang, A. Turansky, SIMS measurement of hydrogen and deuterium detection limits in silicon: comparison of different SIMS instrumentation, J. Vac. Sci. Technol., B: Microelectron. Nanometer Struct.–Process., Meas., Phenom. 34 (2016), https://doi.org/10.1116/1.4940151.

[19] P. Reichart, G. Dollinger, A. Bergmaier, G. Datzmann, A. Hauptner, H.-J. Körner, Sensitive 3D hydrogen microscopy by proton proton scattering, Nucl. Inst. Methods Phys. Res. B 197 (2002) 134–149, https://doi.org/10.1016/S0168-583X(02)01479-9.

[20] P. Reichart, G. Datzmann, A. Hauptner, R. Hertenberger, C. Wild, G. Dollinger, Three-dimensional hydrogen microscopy in diamond, Science 306 (2004) (1979) 1537–1540, https://doi.org/10.1126/science.1102910.

[21] C.M. Welbourn, M.-L.T. Rooney, D.J.F. Evans, A study of diamonds of cube and cube-related shape from the Jwaneng mine, J. Cryst. Growth 94 (1989) 229–252, https://doi.org/10.1016/0022-0248(89)90622-2.

[22] A.R. Lang, Glimpses into the growth history of natural diamonds, J. Cryst. Growth 24–25 (1974), https://doi.org/10.1016/0022-0248(74)90287-5.

[23] Y. Weiss, J. Czas, O. Navon, Fluid inclusions in fibrous diamonds, Diamond: Genesis, Mineralogy and Geochemistry (2023), https://doi.org/10.2138/rmg.2022.88.09.

[24] J.P. Goss, P.R. Briddon, V. Hill, R. Jones, M.J. Rayson, Identification of the structure of the 3107 cm^{-1} H-related defect in diamond, J. Phys. Condens. Matter 26 (2014) 145801, https://doi.org/10.1088/0953-8984/26/14/145801.

[25] F.S. Gentile, S. Salustro, M. Causà, A. Erba, P. Carbonniére, R. Dovesi, The VN3H defect in diamond: a quantum-mechanical characterization, Phys. Chem. Chem. Phys. 19 (2017), https://doi.org/10.1039/c7cp03957c.

[26] D.J.L. Coxon, M. Staniforth, B.G. Breeze, S.E. Greenough, J.P. Goss, M. Monti, J. Lloyd-Hughes, V.G. Stavros, M.E. Newton, An ultrafast shakedown reveals the energy landscape, relaxation dynamics, and concentration of the N_3VH^0 defect in diamond, J. Phys. Chem. Lett. 11 (2020) 6677–6683, https://doi.org/10.1021/acs.jpclett.0c01806.

[27] T. Hainschwang, E. Fritsch, F. Notari, B. Rondeau, A new defect center in type Ib diamond inducing one phonon infrared absorption: the Y center, Diam. Relat. Mater. 21 (2012) 120–126, https://doi.org/10.1016/j.diamond.2011.11.002.

[28] I. Kiflawi, H. Kanda, D. Fisher, S.C. Lawson, The aggregation of nitrogen and the formation of A centres in diamonds, Diam. Relat. Mater. 6 (1997) 1643–1649, https://doi.org/10.1016/S0925-9635(97)00207-0.

[29] E. Fritsch, T. Hainschwang, L. Massi, B. Rondeau, Hydrogen-related optical centers in natural diamond: an update, New Diamond Front. Carbon Technol. 17 (2007).

[30] J.P. Goss, R. Jones, M.I. Heggie, C.P. Ewels, P.R. Briddon, S. Öberg, Theory of hydrogen in diamond, Phys. Rev. B 65 (2002) 115207, https://doi.org/10.1103/PhysRevB.65.115207.

[31] L. Speich, S.C. Kohn, R. Wirth, G.P. Bulanova, C.B. Smith, The relationship between platelet size and the B′ infrared peak of natural diamonds revisited, Lithos 278–281 (2017), https://doi.org/10.1016/j.lithos.2017.02.010.

[32] E.A. Vasilev, D.A. Zedgenizov, I.V. Klepikov, The enigma of cuboid diamonds: the causes of inverse distribution of optical centers within the growth zones, J. Geosci. (2020) 59–70, https://doi.org/10.3190/jgeosci.301.

[33] E. Vasilev, V. Petrovsky, A. Kozlov, A. Antonov, A. Kudryavtsev, K. Orekhova, The story of one diamond: the heterogeneous distribution of the optical centres within a diamond crystal from the Ichetju placer, northern Urals, Mineral. Mag. 83 (2019) 515–522, https://doi.org/10.1180/mgm.2019.32.

[34] S. Salustro, F.S. Gentile, A. Erba, P. Carbonniére, K.E. El-Kelany, R. Dovesi, The characterization of the VNxHy defects in diamond through the infrared vibrational spectrum. A quantum mechanical investigation, Carbon NY 132 (2018), https://doi.org/10.1016/j.carbon.2018.02.045.

[35] S. Salustro, F.S. Gentile, P. D'Arco, B. Civalleri, M. Rérat, R. Dovesi, Hydrogen atoms in the diamond vacancy defect, A quantum mechanical vibrational analysis, Carbon NY 129 (2018) 349–356, https://doi.org/10.1016/j.carbon.2017.12.011.

[36] F. Pascale, S. Salustro, A.M. Ferrari, M. Rérat, P. D'Arco, R. Dovesi, The infrared spectrum of very large (periodic) systems: global versus fragment strategies—the case of three defects in diamond, Theor. Chem. Accounts 137 (2018) 170, https://doi.org/10.1007/s00214-018-2380-3.

[37] E. Fritsch, K. Scarratt, A.T. Collins, R. Messier, J.T. Glass, J.E. Butler, R. Roy, Optical properties of diamonds with an unusually high hydrogen content, in: Materials Research Society International Conference Proceedings. Second International Conference on New Diamond Science and Technology., Washington, DC, 1991, pp. 23–27.

[38] E. Fritsch, K. Scarratt, Gemmological properties of Type Ia diamonds with an unusually high hydrogen content, J. Gemmol. 23 (1993) 451–460.

[39] L. Massi, Etudes des defauts dans les diamants bruns et les diamants riches en hydrogene, PhD Thesis,, University of Nantes, 2006.

[40] T. Hainschwang, F. Notari, G. Pamies, A defect study and classification of Brown diamonds with non-deformation-related color, Minerals 10 (2020) 914, https://doi.org/10.3390/min10100914.

[41] T. Hainschwang, F. Notari, E. Fritsch, L. Massi, Natural, untreated diamonds showing the A, B and C infrared absorptions ("ABC diamonds"), and the H2 absorption, Diam. Relat. Mater. 15 (2006) 1555–1564, https://doi.org/10.1016/j.diamond.2005.12.029.

[42] G.S. Woods, A.T. Collins, Infrared absorption spectra of hydrogen complexes in type I diamonds, J. Phys. Chem. Solids 44 (1983), https://doi.org/10.1016/0022-3697(83)90078-1.

[43] G. Davies, A.T. Collins, P. Spear, Sharp infra-red absorption lines in diamond, Solid State Commun. 49 (1984) 433–436, https://doi.org/10.1016/0038-1098(84)90657-4.

[44] A.M. Zaitsev, Optical Properties of Diamond, Springer Berlin Heidelberg, Berlin, Heidelberg, 2001. doi:https://doi.org/10.1007/978-3-662-04548-0.

[45] B. Dischler, Handbook of Spectral Lines in Diamond (2012), https://doi.org/10.1007/978-3-642-22215-3.

[46] A. Mainwood, Point defects in natural and synthetic diamond: what they can tell us about CVD diamond, Phys. Status Solidi A 172 (1999) 25–35.

[47] A.R. Lang, A.P. Yelisseyev, N.P. Pokhilenko, J.W. Steeds, A. Wotherspoon, Is dispersed nickel in natural diamonds associated with cuboid growth sectors in diamonds that exhibit a history of mixed-habit growth? J. Cryst. Growth 263 (2004) 575–589, https://doi.org/10.1016/j.jcrysgro.2003.11.116.

[48] C.M. Breeding, W. Wang, Occurrence of the Si–V defect center in natural colorless gem diamonds, Diam. Relat. Mater. 17 (2008) 1335–1344, https://doi.org/10.1016/j.diamond.2008.01.075.

[49] S. Eaton-Magaña, T. Ardon, A.M. Zaitsev, Inclusion and point defect characteristics of Marange graphite-bearing diamonds after high temperature annealing, Diam. Relat. Mater. 71 (2017) 20–29, https://doi.org/10.1016/j.diamond.2016.11.011.

[50] M. Wojdyr, Fityk: a general-purpose peak fitting program, J. Appl. Crystallogr. 43 (2010) 1126–1128, https://doi.org/10.1107/S0021889810030499.

[51] A. Erba, J.K. Desmarais, S. Casassa, B. Civalleri, L. Donà, I.J. Bush, B. Searle, L. Maschio, L. Edith-Daga, A. Cossard, C. Ribaldone, E. Ascrizzi, N.L. Marana, J.-P. Flament, B. Kirtman, CRYSTAL23: a program for computational solid state physics and chemistry, J. Chem. Theory Comput. (2022), https://doi.org/10.1021/acs.jctc.2c00958.

[52] R. Dovesi, V.R. Saunders, C. Roetti, R. Orlando, C.M. Zicovich-Wilson, F. Pascale, B. Civalleri, K. Doll, N.M. Harrison, I.J. Bush, Ph. D'Arco, M. Llunell, M. Causa, Y. Noeul, L. Maschio, A. Erba, M. Rerat, S. Casassa, B.G. Searle, J.K. Desmarias, CRYSTAL23 User's Manual (University of Torino), 2023.

[53] P. Giannozzi, S. Baroni, N. Bonini, M. Calandra, R. Car, C. Cavazzoni, D. Ceresoli, G.L. Chiarotti, M. Cococcioni, I. Dabo, A. Dal Corso, S. de Gironcoli, S. Fabris, G. Fratesi, R. Gebauer, U. Gerstmann, C. Gougoussis, A. Kokalj, M. Lazzeri, L. Martin-Samos, N. Marzari, F. Mauri, R. Mazzarello, S. Paolini, A. Pasquarello, L. Paulatto, C. Sbraccia, S. Scandolo, G. Sclauzero, A.P. Seitsonen, A. Smogunov, P. Umari, R.M. Wentzcovitch, QUANTUM ESPRESSO: a modular and open-source software project for quantum simulations of materials, J. Phys. Condens. Matter 21 (2009) 395502, https://doi.org/10.1088/0953-8984/21/39/395502.

[54] P. Giannozzi, O. Andreussi, T. Brumme, O. Bunau, M. Buongiorno Nardelli, M. Calandra, R. Car, C. Cavazzoni, D. Ceresoli, M. Cococcioni, N. Colonna, I. Carnimeo, A. Dal Corso, S. de Gironcoli, P. Delugas, R.A. DiStasio, A. Ferretti, A. Floris, G. Fratesi, G. Fugallo, R. Gebauer, U. Gerstmann, F. Giustino, T. Gorni, J. Jia, M. Kawamura, H.-Y. Ko, A. Kokalj, E. Küçükbenli, M. Lazzeri, M. Marsili, N. Marzari, F. Mauri, N.L. Nguyen, H.-V. Nguyen, A. Otero-de-la-Roza, L. Paulatto, S. Poncé, D. Rocca, R. Sabatini, B. Santra, M. Schlipf, A.P. Seitsonen, A. Smogunov, I. Timrov, T. Thonhauser, P. Umari, N. Vast, X. Wu, S. Baroni, Advanced capabilities for materials modelling with quantum ESPRESSO, J. Phys. Condens. Matter 29 (2017) 465901, https://doi.org/10.1088/1361-648X/aa8f79.

[55] X. Gonze, J.-M. Beuken, R. Caracas, F. Detraux, M. Fuchs, G.-M. Rignanese, L. Sindic, M. Verstraete, G. Zerah, F. Jollet, M. Torrent, A. Roy, M. Mikami, Ph. Ghosez, J.-Y. Raty, D.C. Allan, First-principles computation of material properties: the ABINIT software project, Comput. Mater. Sci. 25 (2002) 478–492, https://doi.org/10.1016/S0927-0256(02)00325-7.

[56] J.L. Duncan, D.C. McKean, I. Torto, A. Brown, A.M. Ferguson, Infrared studies of CH and CD stretching anharmonicity, J. Chem. Soc. Faraday Trans. 2 (84) (1988) 1423, https://doi.org/10.1039/f29888401423.

[57] M.L. Myrick, A.E. Greer, A.A. Nieuwland, R.J. Priore, J. Scaffidi, D. Andreatta, P. Colavita, Birge–Sponer estimation of the C–H bond dissociation energy in chloroform using infrared, near-infrared, and visible absorption spectroscopy. An experiment in physical chemistry, J. Chem. Educ. 85 (2008) 1276. doi:https://doi.org/10.1021/ed085p1276.

[58] J.J. Charette, Le spectre infra-rouge a grande dispersion des trois types de diamants et ses variations en fonction de la temperature, Physica 25 (1959) 1303–1312, https://doi.org/10.1016/0031-8914(59)90053-9.

[59] W.A. Runciman, T. Carter, High resolution infra-red spectra of diamond, Solid State Commun. 9 (1971) 315–317, https://doi.org/10.1016/0038-1098(71)90001-9.

[60] F. De Weerdt, Y.N. Palyanov, A.T. Collins, Absorption spectra of hydrogen in 13C diamond produced by high-pressure, high-temperature synthesis, J. Phys. Condens. Matter 15 (2003) 3163–3170, https://doi.org/10.1088/0953-8984/15/19/316.

[61] I. Kiflawi, D. Fisher, H. Kanda, G. Sittas, The creation of the 3107 cm^{-1} hydrogen absorption peak in synthetic diamond single crystals, Diam. Relat. Mater. 5 (1996) 1516–1518, https://doi.org/10.1016/S0925-9635(96)00568-7.

[62] F. De Weerdt, A.T. Collins, Optical study of the annealing behaviour of the 3107 cm^{-1} defect in natural diamonds, Diam. Relat. Mater. 15 (2006) 593–596, https://doi.org/10.1016/j.diamond.2006.01.005.

[63] S.J. Charles, J.E. Butler, B.N. Feygelson, M.E. Newton, D.L. Carroll, J.W. Steeds, H. Darwish, C.-S. Yan, H.K. Mao, R.J. Hemley, Characterization of nitrogen doped chemical vapor deposited single crystal diamond before and after high pressure, high temperature annealing, Phys. Status Solidi A 201 (2004) 2473–2485, https://doi.org/10.1002/pssa.200405175.

[64] S. Liggins, M.E. Newton, J.P. Goss, P.R. Briddon, D. Fisher, Identification of the dinitrogen (001) split interstitial H1a in diamond, Phys. Rev. B 81 (2010) 085214, https://doi.org/10.1103/PhysRevB.81.085214.

[65] G.L. Melton, T. Stachel, R.A. Stern, J. Carlson, J.W. Harris, Infrared spectral and carbon isotopic characteristics of micro- and macro-diamonds from the Panda kimberlite (Central Slave Craton, Canada), Lithos 177 (2013), https://doi.org/10.1016/j.lithos.2013.06.019.

[66] H. Kanda, K. Watanabe, Distribution of the cobalt-related luminescence center in HPHT diamond, Diam. Relat. Mater. 6 (1997) 708–711, https://doi.org/10.1016/S0925-9635(96)00666-8.

[67] H. Kanda, K. Watanabe, Distribution of nickel related luminescence centers in HPHT diamond, Diam. Relat. Mater. 8 (1999) 1463–1469, https://doi.org/10.1016/S0925-9635(99)00070-9.

[68] V.A. Nadolinny, V.S. Shatsky, O.P. Yuryeva, M.I. Rakhmanova, A. Yu. Komarovskikh, A.A. Kalinin, Yu.N. Palyanov, Formation features of N3V centers in diamonds from the Kholomolokh placer in the northeast Siberian craton, Phys. Chem. Miner. 47 (2020) 4, https://doi.org/10.1007/s00269-019-01070-w.

[69] G.S. Woods, Platelets and the infrared absorption of type Ia diamonds., Proc. R. Soc. Lond. A. 407 (1986). doi:https://doi.org/10.1098/rspa.1986.0094.

[70] I. Kiflawi, J. Bruley, The nitrogen aggregation sequence and the formation of voidites in diamond, Diam. Relat. Mater. 9 (2000) 87–93, https://doi.org/10.1016/S0925-9635(99)00265-4.

[71] Z. Song, J. Su, W. Zhu, T. Lu, Y. Wang, S. He, Spectroscopic study of the 3107 cm^{-1} and 3143 cm^{-1} H-related defects in type Ib diamonds, Crystals (Basel) 12 (2022) 1352, https://doi.org/10.3390/cryst12101352.

[72] M.Y. Lai, C.M. Breeding, T. Stachel, R.A. Stern, Spectroscopic features of natural and HPHT-treated yellow diamonds, Diam. Relat. Mater. 101 (2020) 107642, https://doi.org/10.1016/j.diamond.2019.107642.

[73] A.T. Collins, H. Kanda, H. Kitawaki, Colour changes produced in natural brown diamonds by high-pressure, high-temperature treatment, Diam. Relat. Mater. 9 (2000) 113–122, https://doi.org/10.1016/S0925-9635(00)00249-1.

[74] A. Mainwood, Nitrogen and nitrogen-vacancy complexes and their formation in diamond, Phys. Rev. B 49 (1994), https://doi.org/10.1103/PhysRevB.49.7934.

[75] T. Evans, Z. Qi, The kinetics of the aggregation of nitrogen atoms in diamond, Proc. R. Soc. Lond. A Math. Phys. Sci. 381 (1982) 159–178.

[76] W.R. Taylor, D. Canil, H. Judith Milledge, Kinetics of Ib to IaA nitrogen aggregation in diamond, Geochim. Cosmochim. Acta 60 (1996) 4725–4733, https://doi.org/10.1016/S0016-7037(96)00302-X.

[77] T. Gu, S. Ritterbex, T. Tsuchiya, W. Wang, Novel configurations of VN4 and VN4H defects in diamond platelets: structure, energetics and vibrational properties, Diam. Relat. Mater. 108 (2020) 107957, https://doi.org/10.1016/j.diamond.2020.107957.

[78] W. Wang, T. Moses, R.C. Linares, J.E. Shigley, M. Hall, J.E. Butler, Gem-quality synthetic diamonds grown by a chemical vapor deposition (CVD) method, Gems Gemol. 39 (2003) 268–283.

[79] W. Wang, A. Tallaire, M.S. Hall, T.M. Moses, J. Achard, R.S. Sussmann, A. Gicquel, Experimental CVD synthetic diamonds from LIMHP-CNRS, France, Gems Gemol. 41 (2005) 234–244.

[80] P.M. Martineau, S.C. Lawson, A.J. Taylor, S.J. Quinn, D.J. Evans, M.J. Crowder, Identification of synthetic diamond grown using chemical vapor deposition (CVD), Gems Gemol. 40 (2004) 2–25.

[81] R.U.A. Khan, P.M. Martineau, B.L. Cann, M.E. Newton, D.J. Twitchen, Charge transfer effects, thermo and photochromism in single crystal CVD synthetic diamond, J. Phys. Condens. Matter 21 (2009) 364214, https://doi.org/10.1088/0953-8984/21/36/364214.

[82] J.B. Miller, D.W. Brown, Properties of photochemically modified diamond films, Diam. Relat. Mater. 4 (1995) 435–440, https://doi.org/10.1016/0925-9635(94)05209-3.

[83] T. Hainschwang, D. Simic, E. Fritsch, B. Deljanin, S. Woodring, N. DelRe, Chameleon diamonds, Gems Gemol. 41 (2005) 20–35.

[84] S. Satoh, H. Sumiya, K. Tsuji, S. Yazu, Difference in Nitrogen Concentration and Aggregation among (111) and (110) Growth Sectors of Large Synthetic Diamonds, in: S. et al. Saito (Ed.), Science and Technology of New Diamond, Terra Scientific Publishing, 1990: pp. 351–355.

[85] C.V. Peaker, First Principles Study of Point Defects in Diamond, Newcastle University, PhD, 2018.

[86] A. Stacey, T.J. Karle, L.P. McGuinness, B.C. Gibson, K. Ganesan, S. Tomljenovic-Hanic, A.D. Greentree, A. Hoffman, R.G. Beausoleil, S. Prawer, Depletion of nitrogen-vacancy color centers in diamond via hydrogen passivation, Appl. Phys. Lett. 100 (2012), https://doi.org/10.1063/1.3684612.

[87] M.N.R. Ashfold, J.P. Goss, B.L. Green, P.W. May, M.E. Newton, C.V. Peaker, Nitrogen in diamond, Chem. Rev. 120 (2020) 5745–5794, https://doi.org/10.1021/acs.chemrev.9b00518.

[88] T. Hainschwang, E. Fritsch, F. Notari, B. Rondeau, A. Katrusha, The origin of color in natural C center bearing diamonds, Diam. Relat. Mater. 39 (2013) 27–40, https://doi.org/10.1016/j.diamond.2013.07.007.

[89] E. Fritsch, L. Massi, G.R. Rossman, T. Hainschwang, S. Jobic, R. Dessapt, Thermochromic and photochromic behaviour of "chameleon" diamonds, Diam. Relat. Mater. 16 (2007) 401–408, https://doi.org/10.1016/j.diamond.2006.08.014.

[90] T. Hainschwang, F. Notari, G. Pamies, A defect study and classification of Brown diamonds with deformation-related color, Minerals 10 (2020) 903, https://doi.org/10.3390/min10100903.